Electronic Supplementary Material (ESI) for Dalton Transactions.
This journal is © The Royal Society of Chemistry 2022

Electronic Supplementary Information

A Porphyrin(2.1.2.1) Bis-boron Complex as Deep-red AIE Luminophore Induced by Intermolecular F-π Interaction

Ningchao Liu,[a] Xiaojuan Lv,[a] Bentian Xiao,[a] Daiki Kuzuhara,*[b] Peifeng Mei,[c] Naoki Aratani,[c] Hiroko Yamada,[c] Fengxian Qiu,*[a] Jianming Pan,*[a] and Songlin Xue*[a]

[a]School of Chemistry and Chemical Engineering, Jiangsu University, Zhenjiang 212013, China

[b]Faculty of Science and Engineering, Iwate University, 4-3-5 Ueda, Morioka 020-8551, Japan

[c]Division of Materials Science, Nara Institute of Science and Technology (NAIST), 8916-5 Takayama-cho, Ikoma, Nara 630-0192, Japan

1. Instruments, materials, and theoretical calculations

All solvents and chemicals were reagent grade quality, obtained commercially, and used without further purification except as noted. ^{1}H NMR, ^{13}C NMR, and ^{19}F NMR spectra were recorded on a JNM-ECX 400 spectrometer (operating as 400 MHz for ^{1}H, 100 MHz for ^{13}C, and 376 MHz for ^{19}F) using the residual solvent as the internal reference for ^{1}H (δ = 7.26 ppm in $CDCl_3$), ^{13}C (δ = 76.8 ppm in $CDCl_3$) and CF_3COOH as the external reference for ^{19}F (δ = -76.5 ppm). HR-MALDI-TOF mass spectrum was recorded on a Bruker Daltonics autoflex MALDI-TOF MS spectrometer. The UV-Vis absorption spectra were measured with a JASCO UV/VIS/NIR Spectrophotometer V-670. The fluorescence spectra of boron complexes in solution, solid state, and aggregated particles in THF/H_2O were measured with a JASCO PL spectrofluorometer FP-6600. Fluorescence lifetimes were recorded on Picosecond Fluorescence Lifetime Measurement System C4780. The fluorescence quantum yields were recorded on an Absolute PL Quantum Yield Measurement System C9920-02 (Hamamatsu). The aggregated particles in THF/H_2O were prepared by the addition of H_2O into the solution of boron complexes in THF. The cyclic voltammetry was conducted in a solution of 0.1 M tetrabutylammonium perchlorate (TBAP) in dry-CH_2Cl_2 with a scan rate of 0.1 V s^{-1} in an argon-filled cell. A glassy carbon electrode and a platinum wire were used as a working and a counter electrodes. A saturated Calomel electrode (SCE) was used as reference electrodes. All density functional theory calculations were achieved with the Gaussian 09 program package. The geometries of **2a**, **3a**, **2b**, and **3b** were optimized at the Becke's three-parameter hybrid functional combined with the Lee-Yang-Parr correlation functional abbreviated as the B3LYP level of density functional theory with the 6-31G(d, p) level.[1]

2. X-ray Analysis

X-ray crystallographic data for **2a** (CCDC: 2122758), **3a** (CCDC: 2105609), **2b** (CCDC: 2105610), and **3b** (CCDC: 2107596) complexes were recorded at 297 K and 193 K on a Rigaku R-AXIS RAPID/S using M_o−K_α radiation from the corresponding set of confocal optics. The structures were solved by direct methods and refined on F^2 by full-matrix least-squares using the CrystalClear and SHELXS−2000 program.[2]

3. Synthesis Work

Synthesis of 1a and 1b

Dipyrrolylbenzene (**DPB**) and dibenzoporphyrins(2.1.2.1) (**1a** and **1b)** were synthesized through our established method.[3]

1a. **DPB** (0.20 g, 1.0 mmol) and benzaldehyde (0.10 g, 1.0 mmol) were dissolved in dry CH_2Cl_2 (50 mL) and bubbled with nitrogen for 5 min, then BF_3•OEt_2 (4.3 mg, 0.03 mmol, 3 mol%) was added to reaction mixture. The reaction mixture was stirred for 3 hours at room temperature under nitrogen in the dark. The DDQ (0.22 g, 1.0 mmol) was added to the reaction mixture, which was stirred for 1 hour. The residue was purified by alumina column chromatography (CH_2Cl_2) and silica gel column chromatography (CH_2Cl_2/MeOH = 20/1), and gave the **1a** (74 mg, 0.13 mmol) in 25% yield. ^{1}H NMR (400 MHz, $CDCl_3$) δ =12.23 (brs, 2H), 7.51 (d, J = 8 Hz, 4H), 7.46-7.39 (m, 14H), 6.51 (d, J = 4 Hz, 4H), 6.27 (d, J = 4 Hz, 4H) ppm. HR-MALDI-TOF-MS: Calcd. For $C_{42}H_{28}N_4$: 588.2308 $[M]^+$, Found: 588.2301. UV-Vis (in CH_2Cl_2) λ [nm] (ε [$M^{-1}cm^{-1}$]): 434 (73300), 492(10100).

1b. **DPB** (0.20 g, 1.0 mmol) and pentafluorobenzaldehyde (0.20 g, 1.0 mmol) were dissolved in dry CH_2Cl_2 (50 mL) and bubbled with nitrogen for 5 min, then BF_3•OEt_2 (4.3 mg, 0.03 mmol, 3 mol%) was added to reaction mixture. The reaction mixture was stirred for 3 hours at room temperature under nitrogen in the dark. The DDQ (0.23 g, 1.0 mmol) was added to the reaction mixture, which was stirred for 1 hour. The residue was purified by alumina column chromatography (CH_2Cl_2) and silica gel column chromatography (CH_2Cl_2/MeOH = 20/1), and gave the **1b** (35 mg, 0.05 mmol) in 9% yield. ^{1}H NMR (400 MHz, $CDCl_3$) δ = 12.18 (brs, 2H), 7.48 (s, 8H), 6.39 (d, J = 4 Hz, 4H), 6.27 (d, J = 4 Hz, 4H) ppm. ^{19}F NMR ($CDCl_3$, 376 MHz, CF_3COOH) δ = -138.04 – -138.19 (m, 2F), -139.02 – -139.12 (m, 2F), -152.61 – -152.72 (m, 2F), -161.12 – -161.42 (m, 4F) ppm. HR-MALDI-TOF-MS: Calcd. For $C_{42}H_{18}F_{10}N_4$: 768.1366 $[M]^+$, Found: 768.1359. UV-Vis (in CH_2Cl_2) λ [nm] (ε [$M^{-1}cm^{-1}$]): 433 (75600), 490 (10500).

Synthesis of 2a and 3a

To a solution of **1a** (60 mg, 0.10 mmol) in toluene (30 mL) and triethylamine (TEA) (0.40 g, 4.0

mmol) was added BF_3•Et_2O (1.4 g, 10 mmol) under argon. After stirring at 80 $_oC$ for 12 h, the reaction mixture was extracted with CH_2Cl_2. The organic phase was washed with aqueous $NaHCO_3$, water, and brine, and dried over Na_2SO_4. After removal of the solvent, the resulting crude product was purified by silica gel column chromatography (CH_2Cl_2) to give **2a** (41 mg, 0.065 mmol) in 65% yield and **3a** (16 mg, 0.02 mmol) in 24% yield. **2a**. ^{1}H NMR (400 MHz, $CDCl_3$) δ =13.16 (brs, 1H), 7.54 (m, J = 24 Hz, 6H), 7.48(d, J = 8Hz, 2H), 7.40 (m, J = 20 Hz, 10H), 6.74 (d, J = 4 Hz, 2H), 6.47 (d, J = 4 Hz, 2H), 6.25 (d, J = 4 Hz, 2H), 6.08 (d, J = 4 Hz, 2H) ppm. ^{13}C NMR (100 MHz, $CDCl_3$) δ = 157.88, 155.07, 141.09, 135.68, 132.60, 130.27, 128.76, 128.49, 128.21, 127.43, 120.65, 117.76 ppm. ^{19}F NMR ($CDCl_3$, 376 MHz, CF_3COOH) δ = -131.06 – -131.62 (m, 1F), -151.21 – -151.492 (m, 1F) ppm. HR-MALDI-TOF-MS: Calcd. For $C_{42}H_{28}BF_2N_4$: 637.2377 [M+H]$^+$, Found: 637.2371. UV-Vis (in CH_2Cl_2) λ [nm] (ε [M^{-1}cm^{-1}]): 459 (79500), 534 (6800). **3a**. ^{1}H NMR (400 MHz, $CDCl_3$) δ = 7.52 (m, J = 20 Hz, 8H), 7.47 (m, J = 20 Hz, 10H), 6.69 (d, J = 4 Hz, 4H), 6.16 (d, J = 4 Hz, 4H) ppm. ^{13}C NMR (100 MHz, $CDCl_3$) δ = 157.16, 145.94, 135.21, 134.54, 133.46, 130.17, 129.62, 128.73, 128.33, 128.08, 127.62, 120.20 ppm. ^{19}F NMR ($CDCl_3$, 376 MHz, CF_3COOH) δ = -128.80 (s, 2F) ppm. HR-MALDI-TOF-MS: Calcd. For $C_{42}H_{26}B_2F_2N_4O$+Na$^+$: 685.2167 [M+Na]$^+$, Found: 685.2162. UV-Vis (in CH_2Cl_2)λ[nm](ε[M^{-1}cm^{-1}]): 475 (89000), 563(6650).

Synthesis of 2b and 3b

To a solution of **1b** (38 mg, 0.05 mmol) in toluene (20 mL) and triethylamine (TEA) (0.20 g, 2.0 mmol) was added BF_3•Et_2O (0.71 g, 5.0 mmol) under argon. After stirring at 80 ^oC for 12 h, the reaction mixture was extracted with CH_2Cl_2. The organic phase was washed with aqueous $NaHCO_3$, water, and brine, and dried over Na_2SO_4. After removal of the solvent, the resulting crude product was purified by silica gel column chromatography (CH_2Cl_2) to give **2b** (25 mg, 0.030 mmol) in 60% yield and **3b** (6.3 mg, 0.0075 mmol) in 15% yield. **2b**. ^{1}H NMR (400 MHz, $CDCl_3$) δ =12.90 (brs, 1H), 7.59 (m, J = 8 Hz, 2H), 7.44 (m, J = 24 Hz, 6H), 6.57 (d, J = 4 Hz, 2H), 6.34 (d, J = 4 Hz, 2H), 6.23 (d, J = 4 Hz, 2H), 6.04 (d, J = 4 Hz, 2H) ppm. ^{13}C NMR (100 MHz, $CDCl_3$) δ = 160.13, 156.37, 140.52, 135.12, 132.00, 128.92, 128.31, 128.16, 127.80, 127.20, 122.00 118.85 ppm. ^{19}F NMR ($CDCl_3$, 376 MHz, CF_3COOH) δ = -130.89 – -131.43 (m, 1F), -137.05 – -137.16 (m, 1F), -137.87 (m, 1F), -138.62 – -138.90 (m, 2F), -150.02– -150.14 (m, 1F), -151.01 – -151.48 (m, 1F), -152.74 – -152.86 (m, 1F), -159.70 – -159.90 (m, 2F), -161.18 – -161.56 (m, 2F) ppm. HR-MALDI-TOF-MS: Calcd. For $C_{42}H_{17}BF_{12}N_4$: 815.1385 [M]$^+$, Found: 815.1380. UV-Vis (in CH_2Cl_2) λ [nm] (ε [M^{-1}cm^{-1}]): 460 (12400), 475 (84600). **3b**. ^{1}H NMR (400 MHz, $CDCl_3$) δ = 7.49 (s, br, 8H), 6.55 (d, J = 4 Hz, 4H), 6.15 (d, J = 4 Hz, 4H) ppm. ^{13}C NMR (100 MHz, $CDCl_3$) δ = 159.06, 135.05, 132.60, 129.10, 128.07, 127.23, 121.40 ppm. ^{19}F NMR ($CDCl_3$, 376 MHz, CF_3COOH) δ = -130.03 (brs, 2F), -136.68 – -136.77 (m, 2F), -137.96 – -138.01 (m, 2F), -150.19 – -150.31 (m, 2F), -159.68 – -159.81 (m, 2F), -160.11 – -160.25 (m, 2F) ppm. HR-MALDI-TOF-MS: Calcd. For $C_{42}H_{16}B_2F_{12}N_4O$+Na$^+$: 863.1283 [$M$+Na]$^+$, Found: 863.1291. UV-Vis (in CH_2Cl_2) λ [nm] (ε [M^{-1}cm^{-1}]): 461 (17400), 486 (100300).

4. Supporting Figures

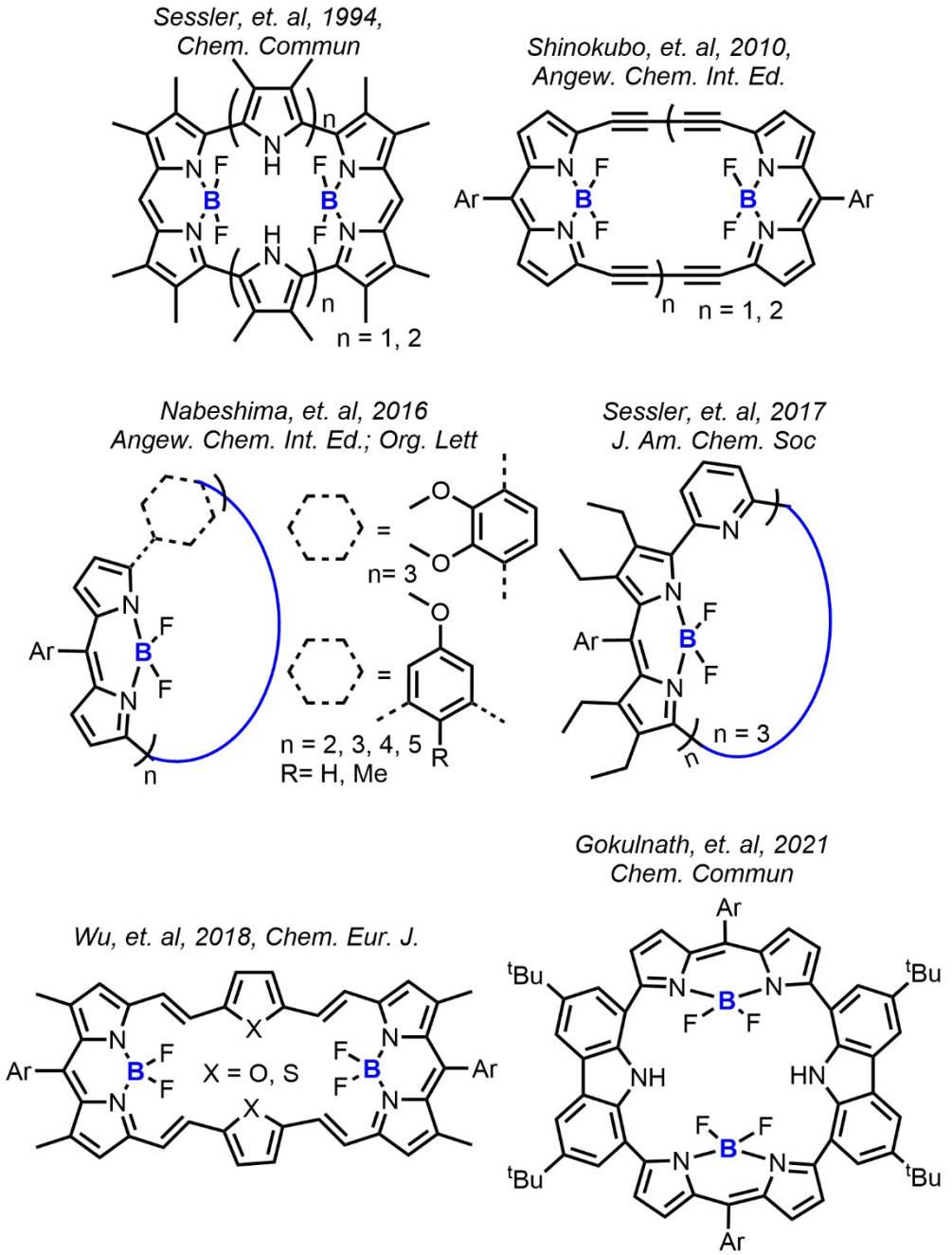

Fig. S1. Reported boron complexes of rigid or flexible expanded porphyrin macrocycles containing various bridging units.

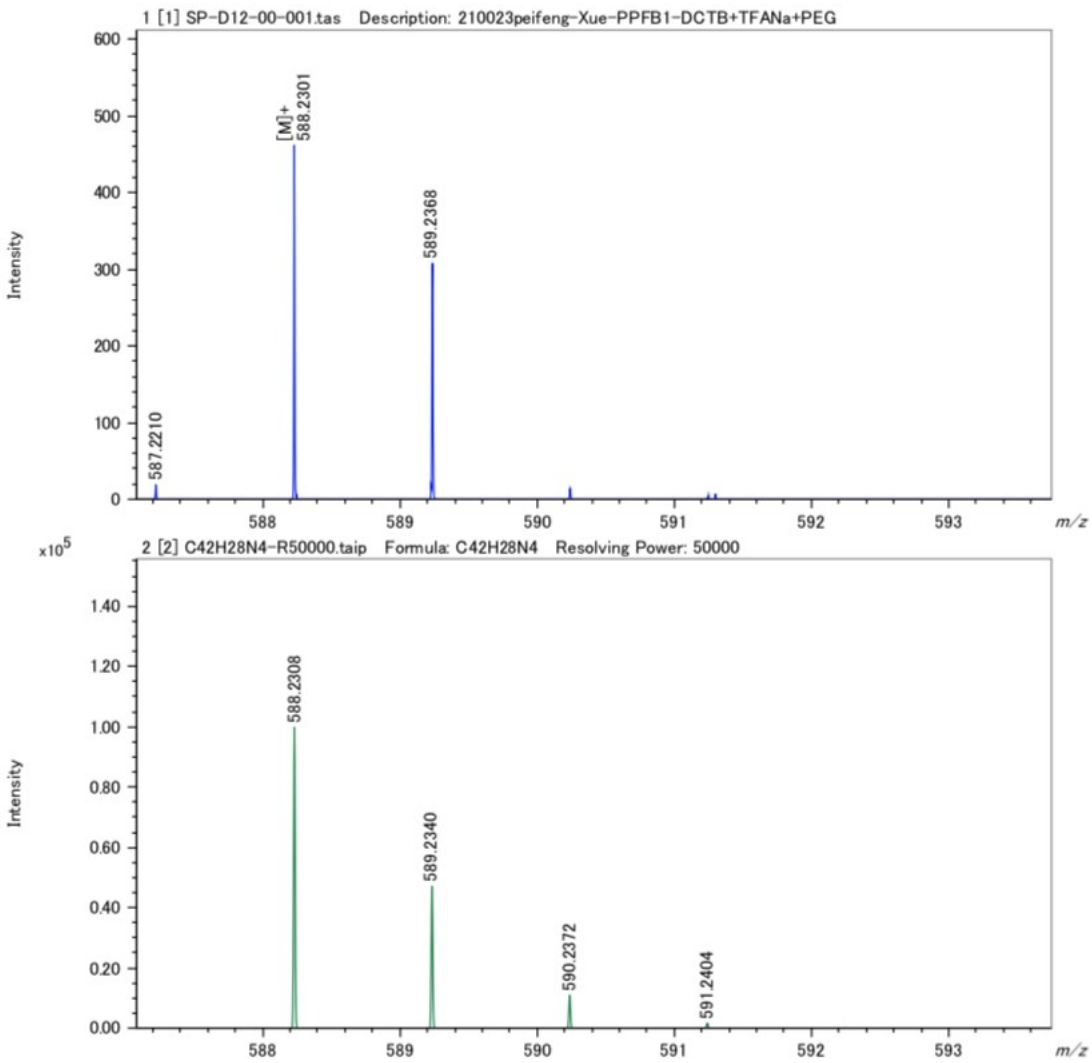

Fig. S2. HR-MALDI-TOF-MS spectrum of **1a**.

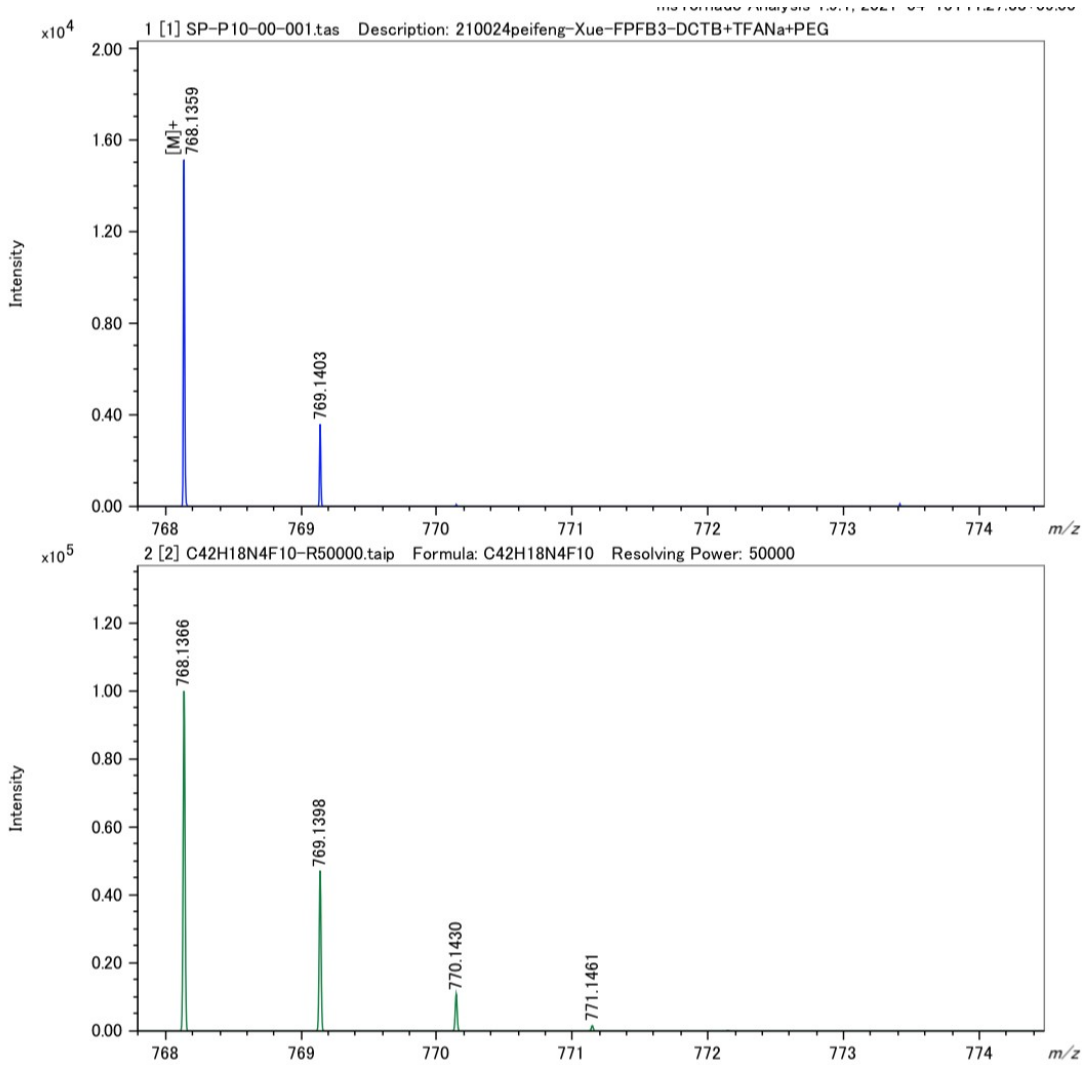

Fig. S3. HR-MALDI-TOF-MS spectrum of **1b**.

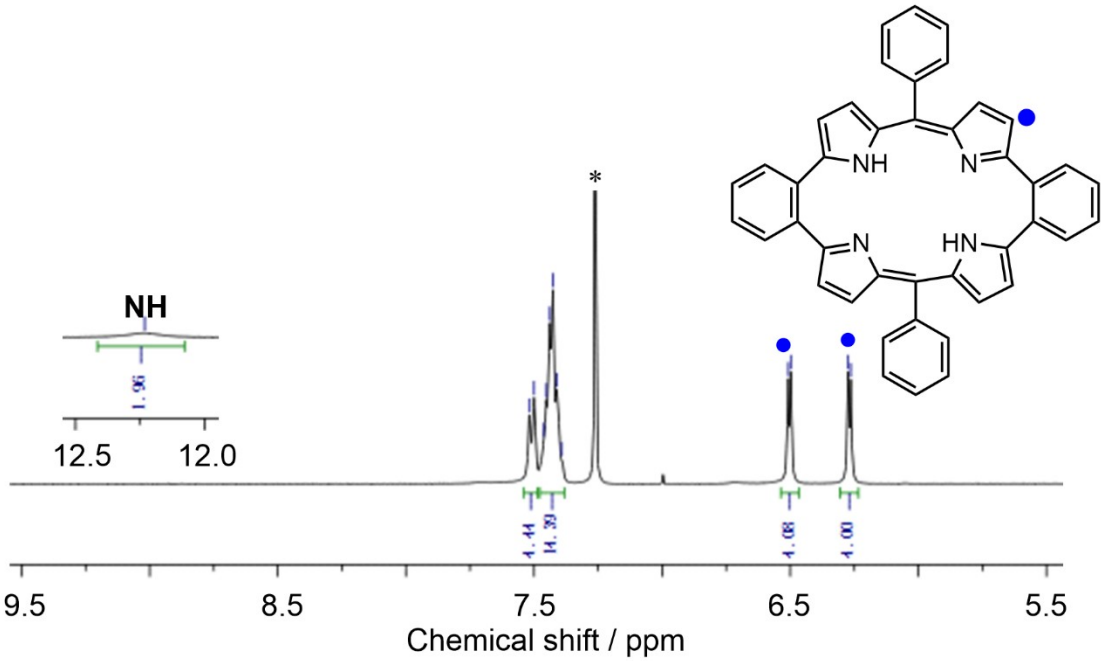

Fig. S4. ^{1}H NMR spectrum of **1a** in $CDCl_3$ at 293 K. The asterisks indicate residual solvent peaks.

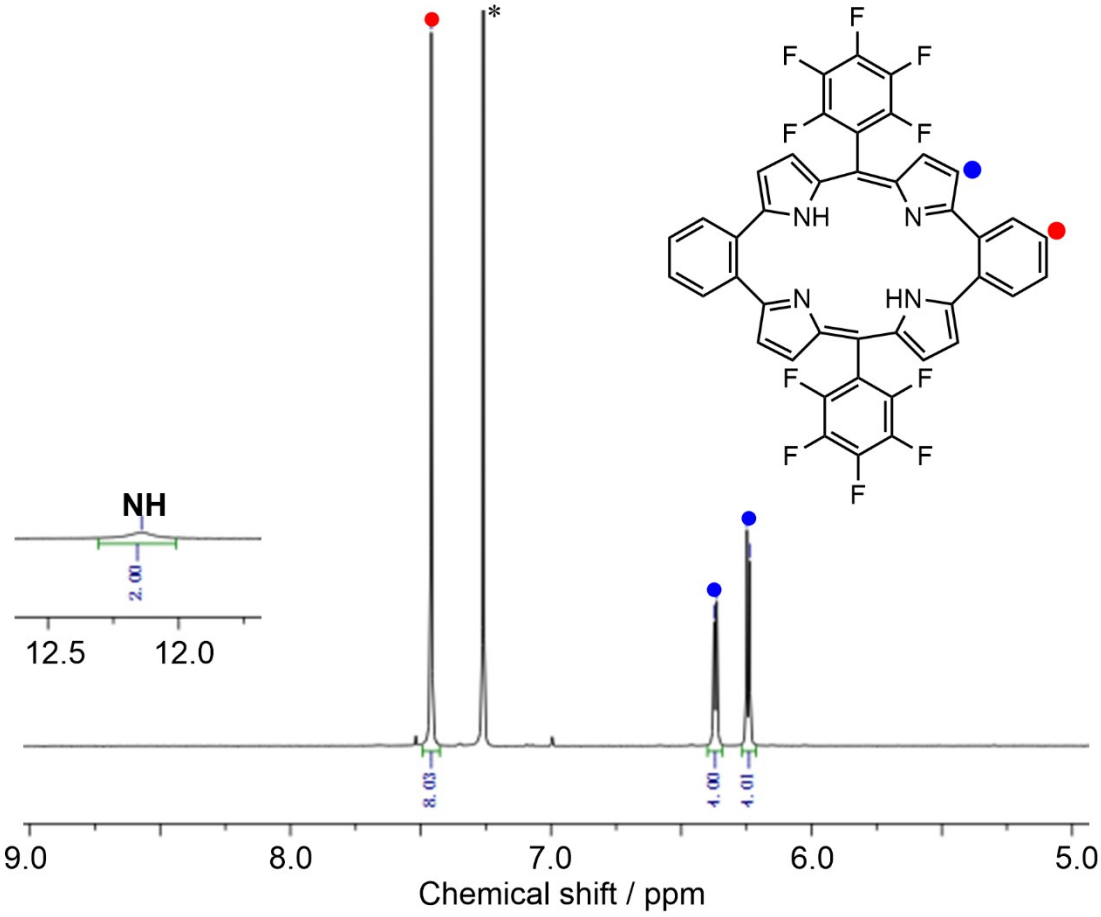

Fig. S5. ^{1}H NMR spectrum of **1b** in $CDCl_3$ at 293 K. The asterisks indicate residual solvent peaks.

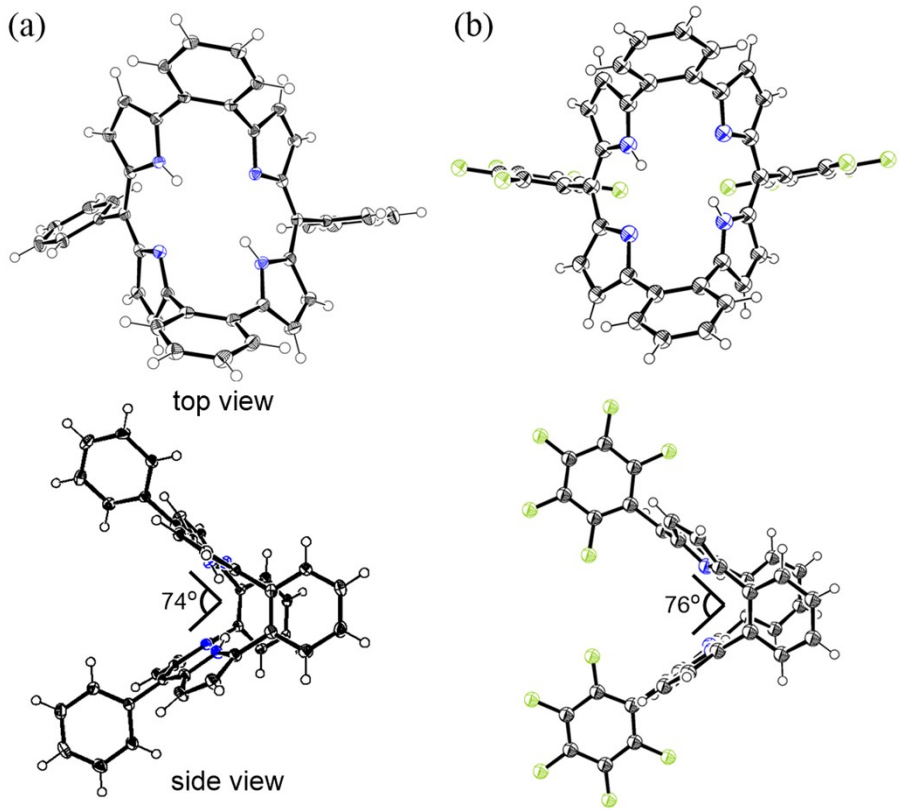

Fig. S6. Crystal structures and angles of (a) **1a** and (b) **1b**. Ellipsoids of crystal structures are set at 50% probability. The data of **1b** was taken from ref. 3c.

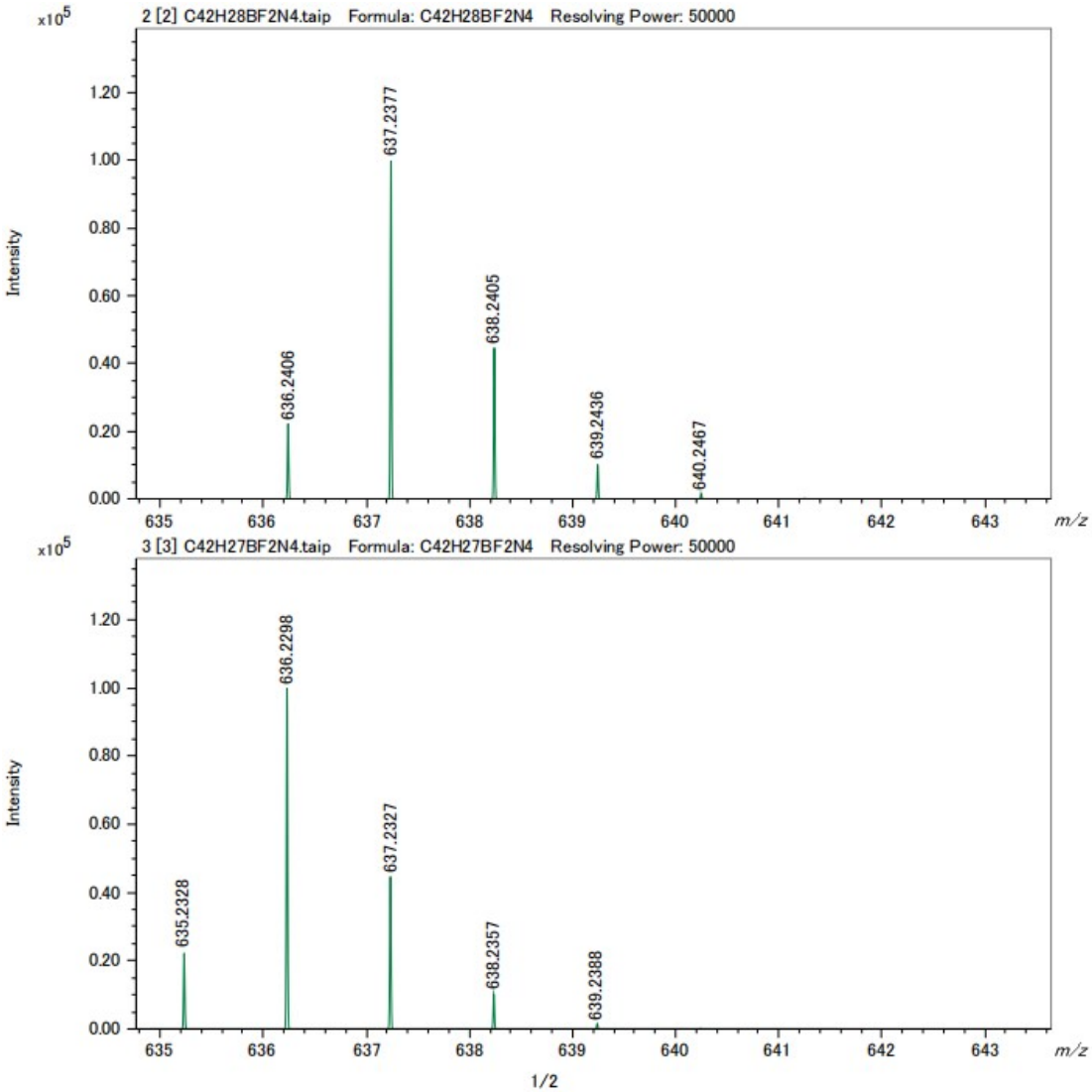

Fig. S7. HR-MALDI-MS spectrum of **2a**.

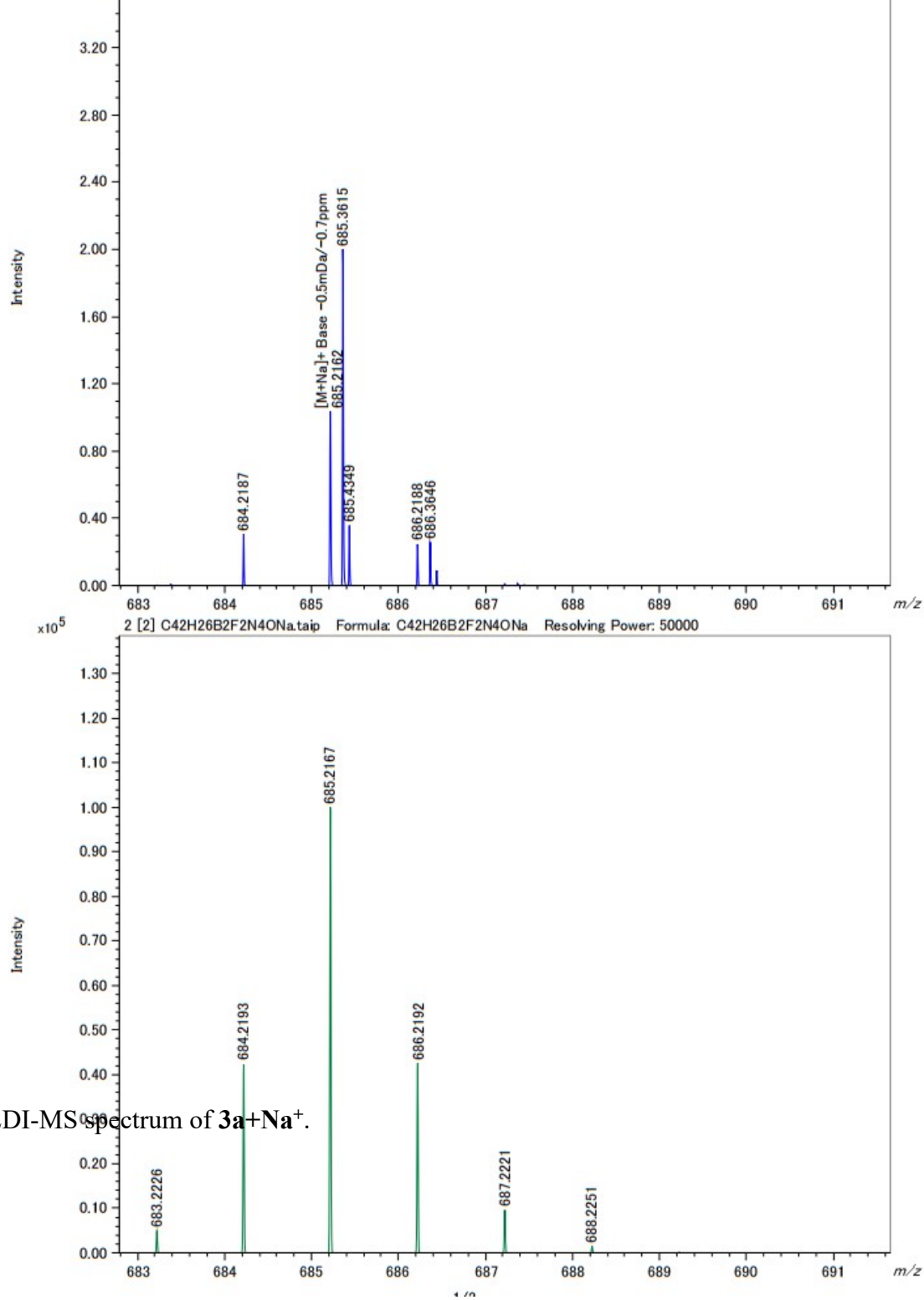

Fig. S8. HR-MALDI-MS spectrum of **3a**+**Na**$^+$.

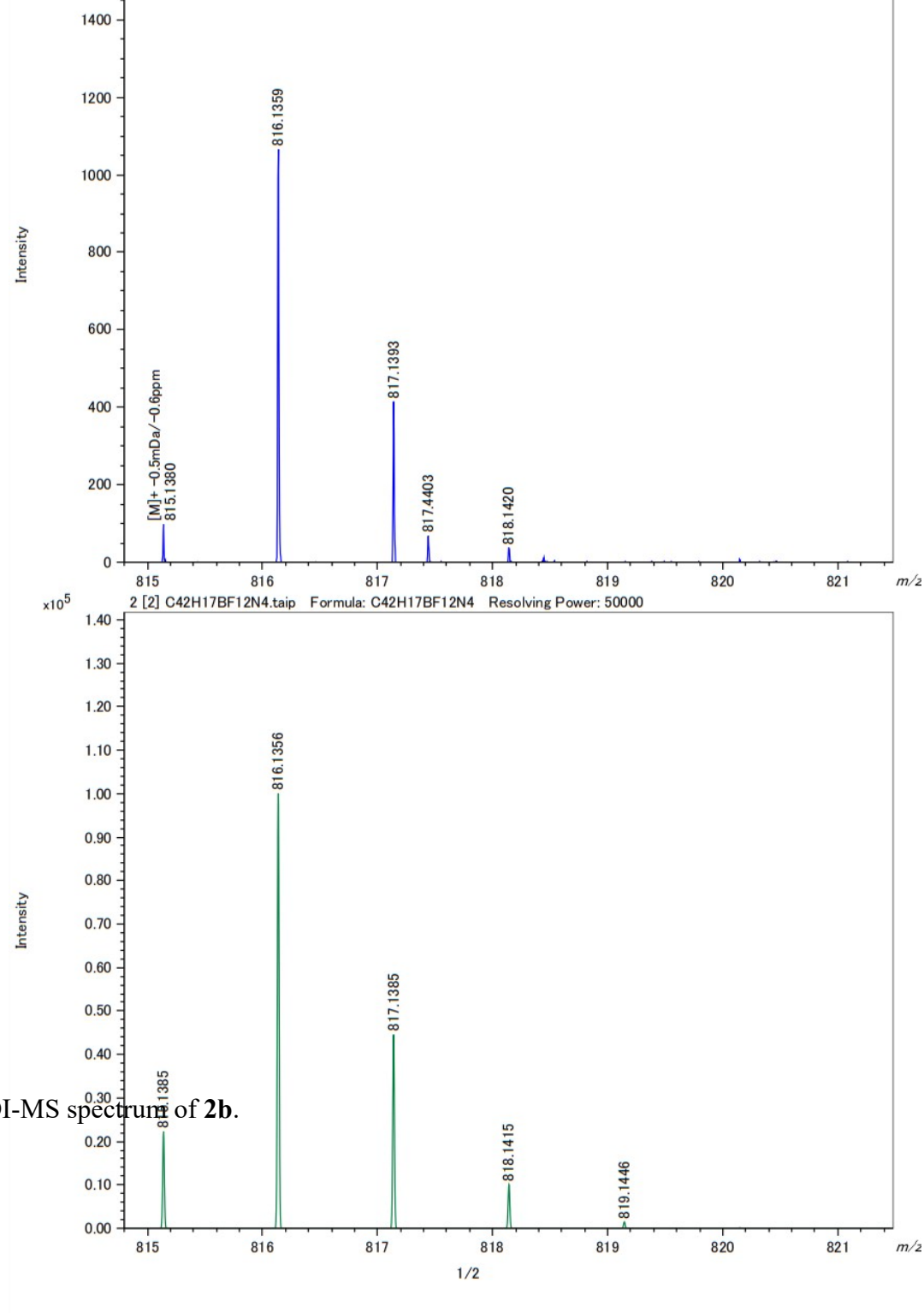

Fig. S9. HR-MALDI-MS spectrum of **2b**.

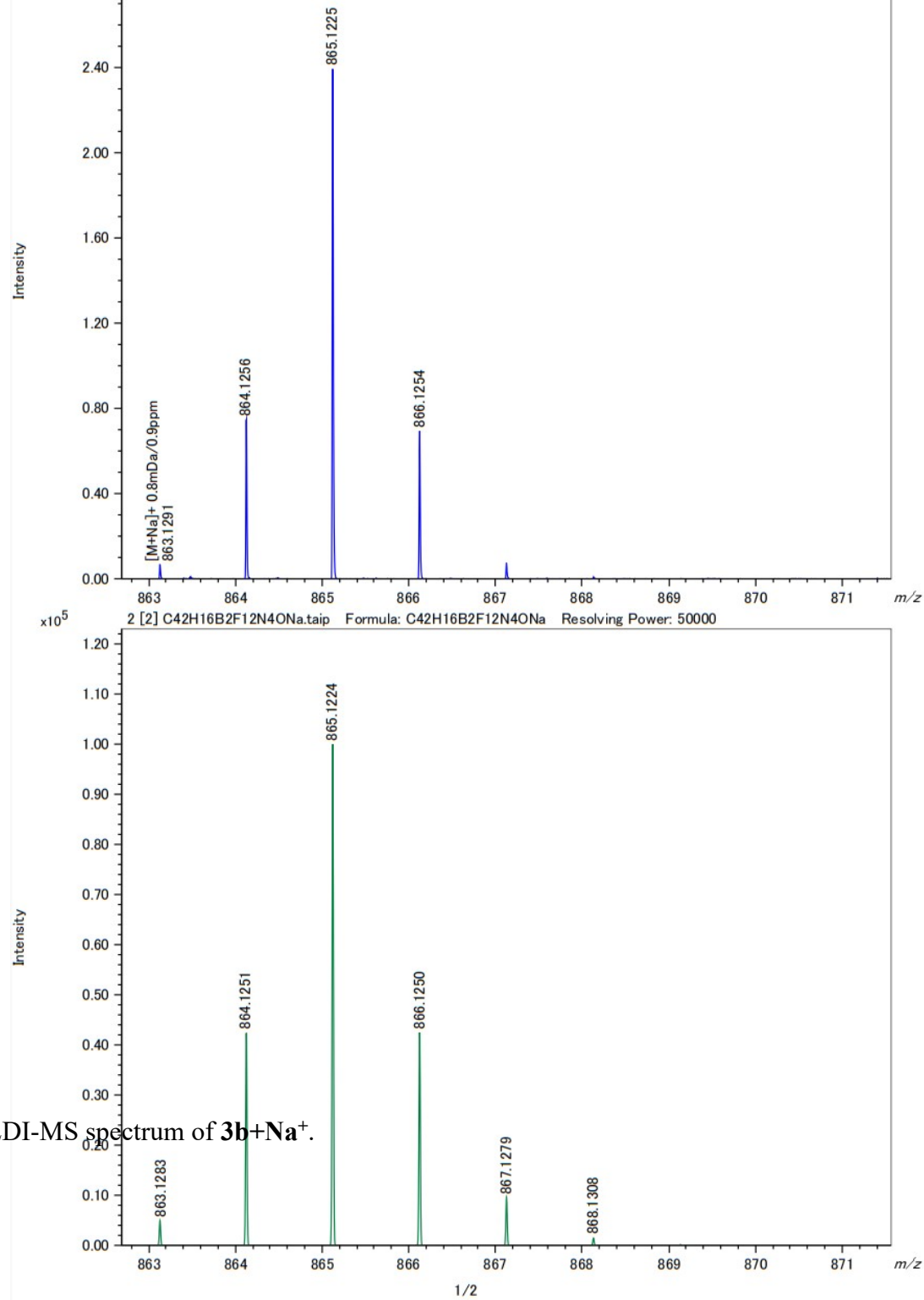

Fig. S10. HR-MALDI-MS spectrum of **3b**+**Na**$^{+}$.

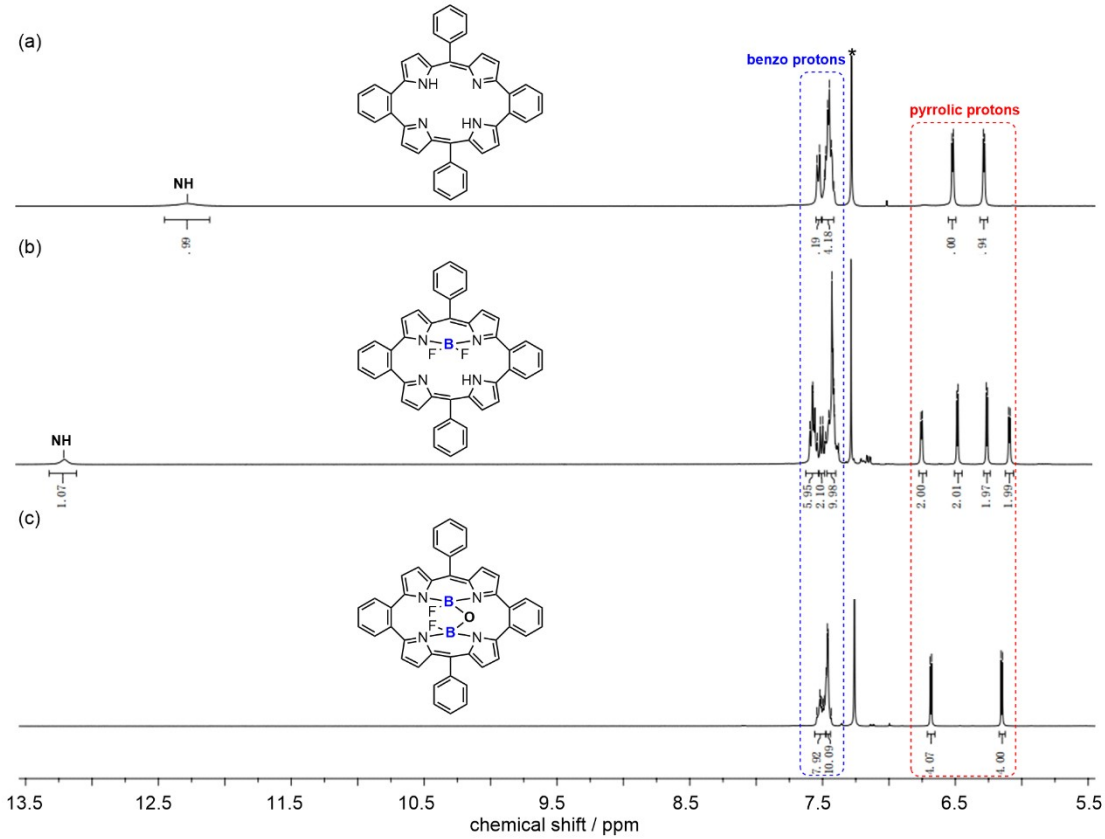

Fig. S11. ^{1}H NMR spectra of (a) **1a**, (b) **2a**, and (c) **3a** in $CDCl_3$ at 293 K. The asterisks indicate residual solvent peaks.

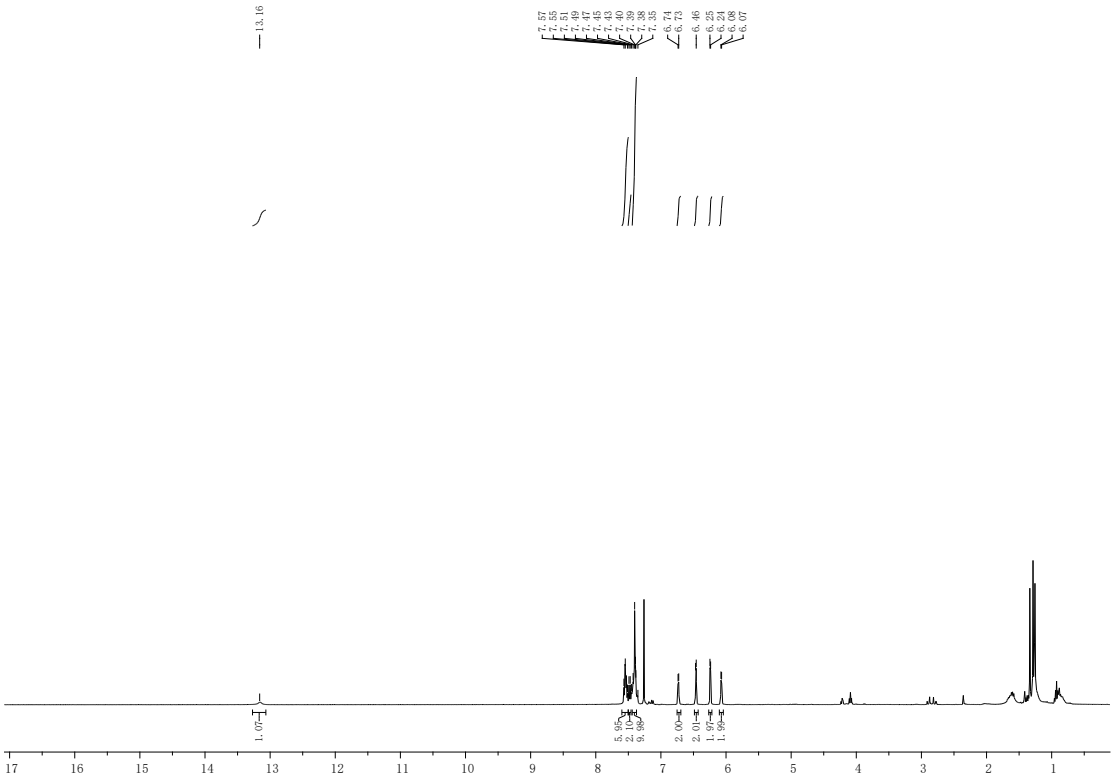

Fig. S12. ^{1}H NMR spectrum of **2a** in $CDCl_3$ at 293 K.

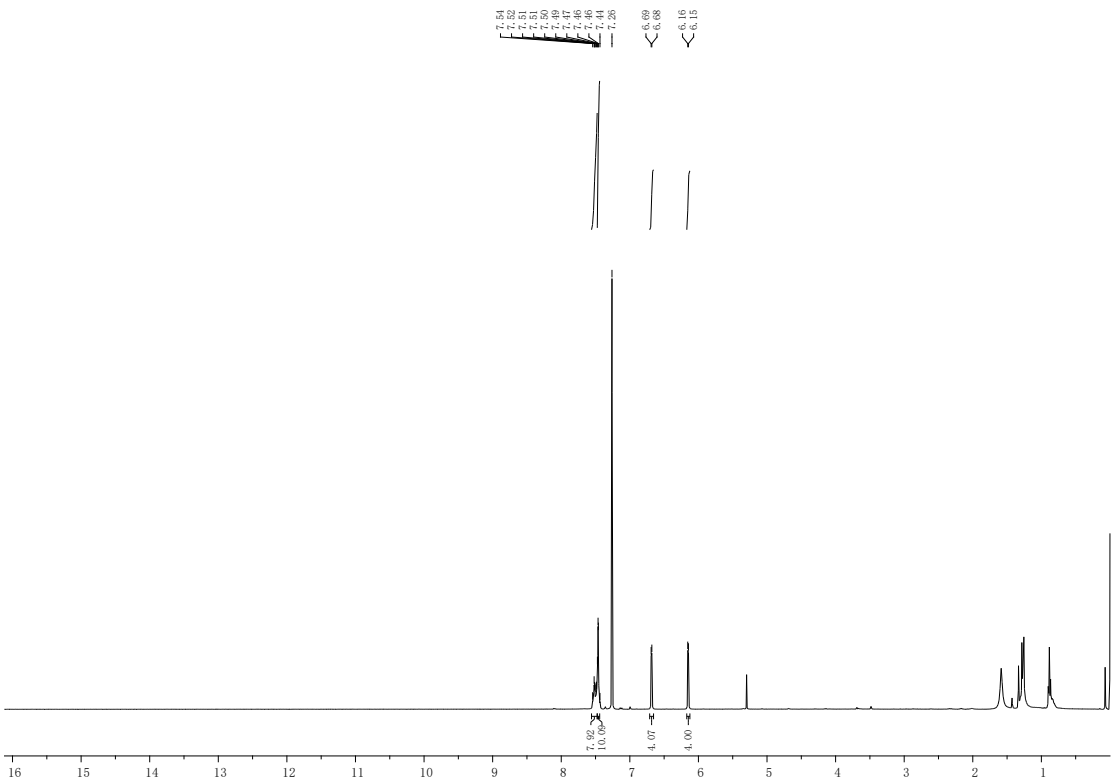

Fig. S13. ^{1}H NMR spectrum of **3a** in $CDCl_3$ at 293 K.

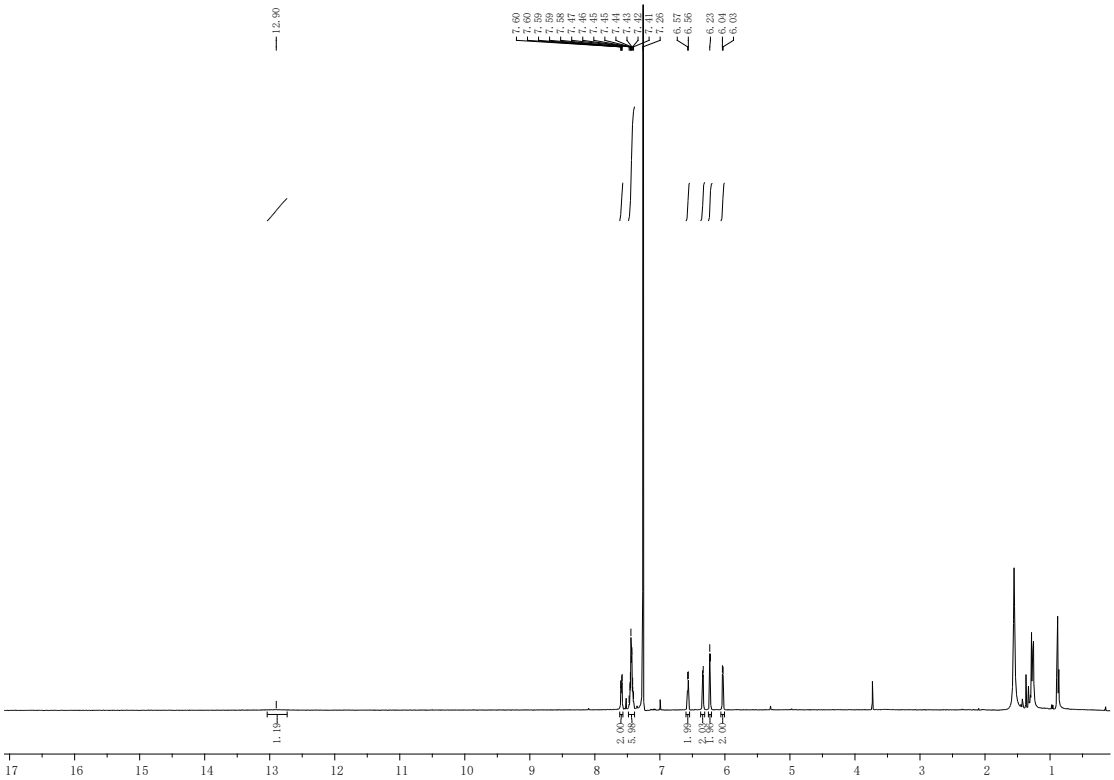

Fig. S14. ^{1}H NMR spectrum of **2b** in $CDCl_3$ at 293 K.

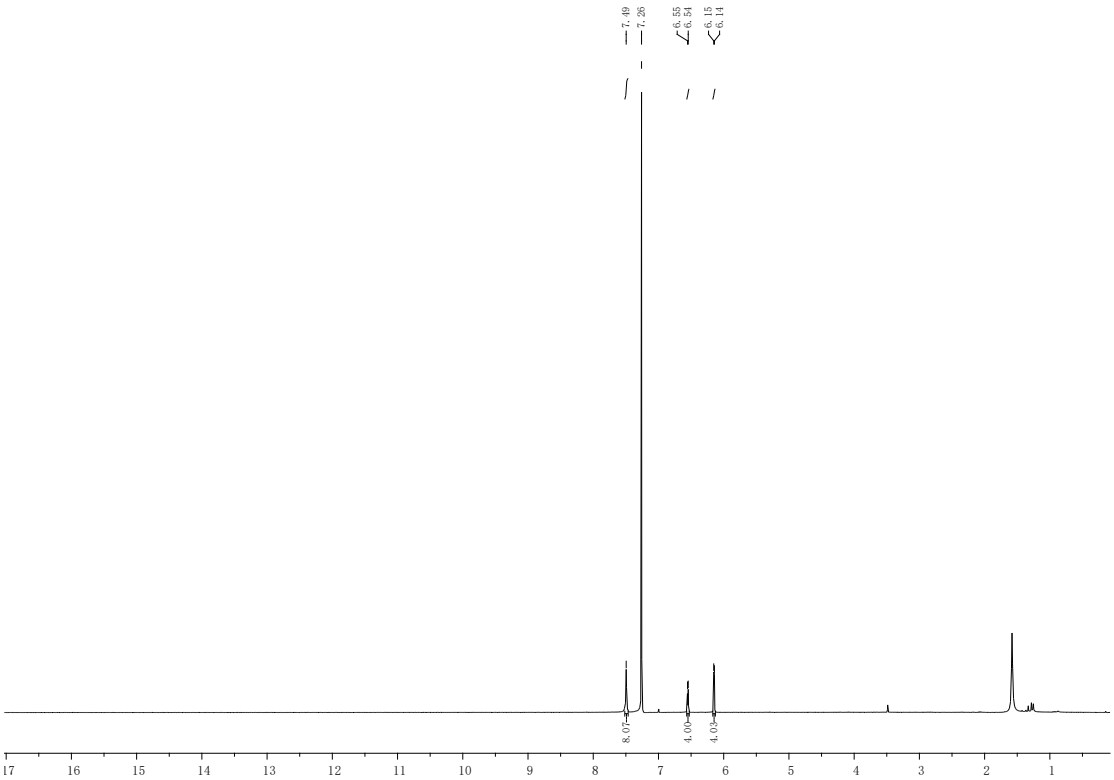

Fig. S15. ^{1}H NMR spectrum of **3b** in $CDCl_3$ at 293 K.

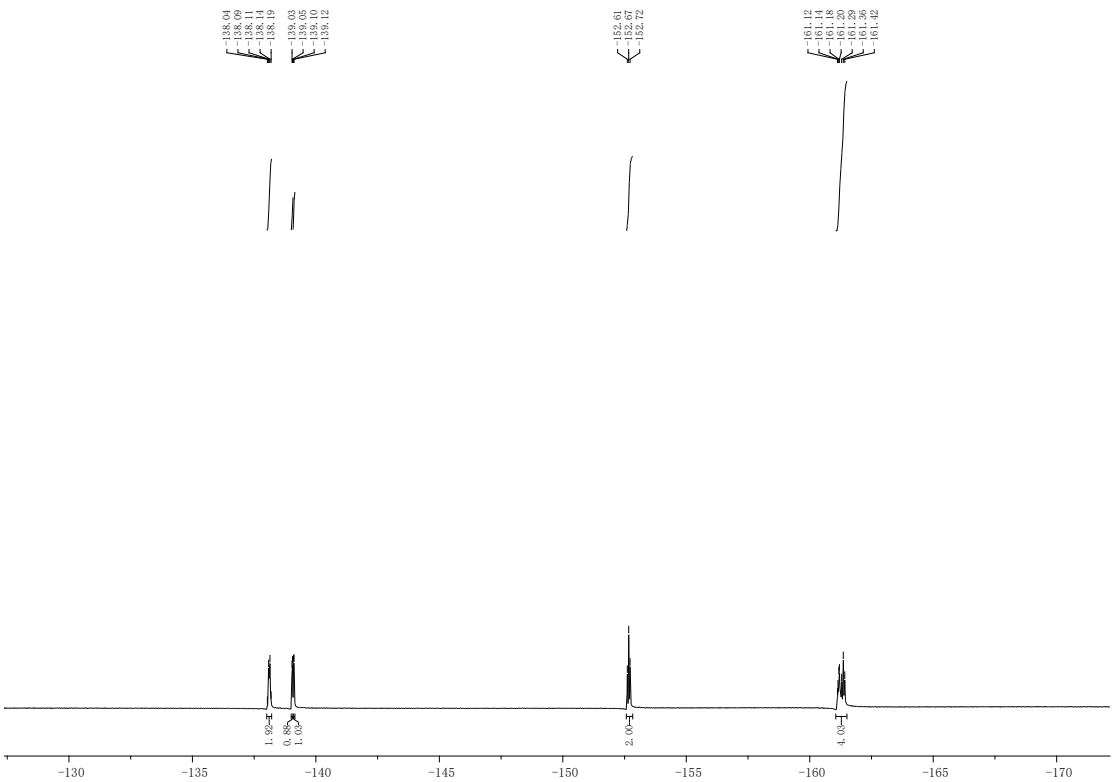

Fig. S16. ^{19}F NMR spectrum **1b** in $CDCl_3$ at 293 K.

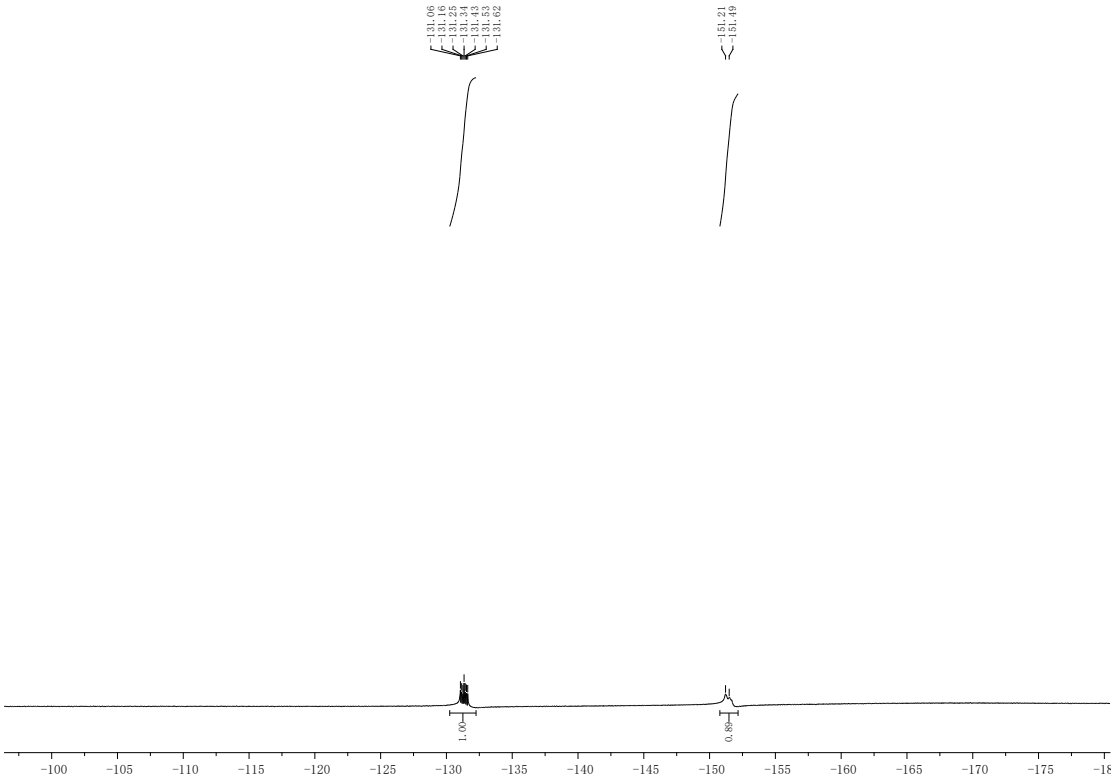

Fig. S17. ^{19}F NMR spectrum of **2a** in $CDCl_3$ at 293 K.

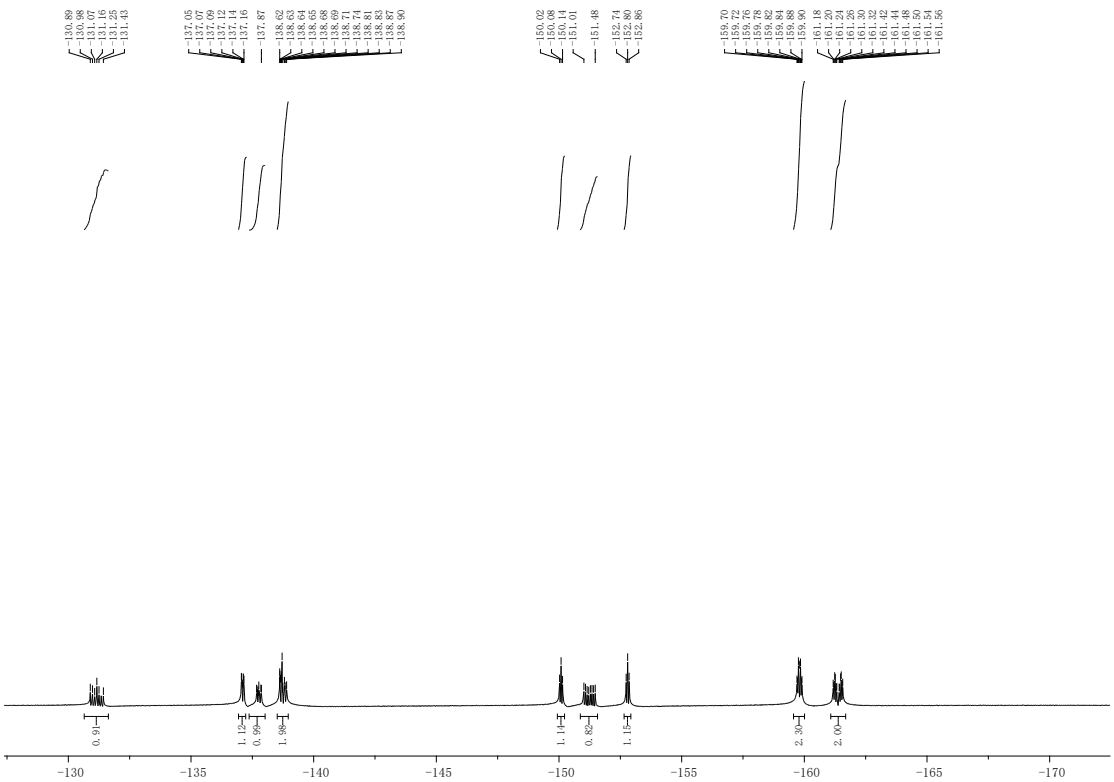

Fig. S18. ^{19}F NMR spectrum of **2b** in $CDCl_3$ at 293 K.

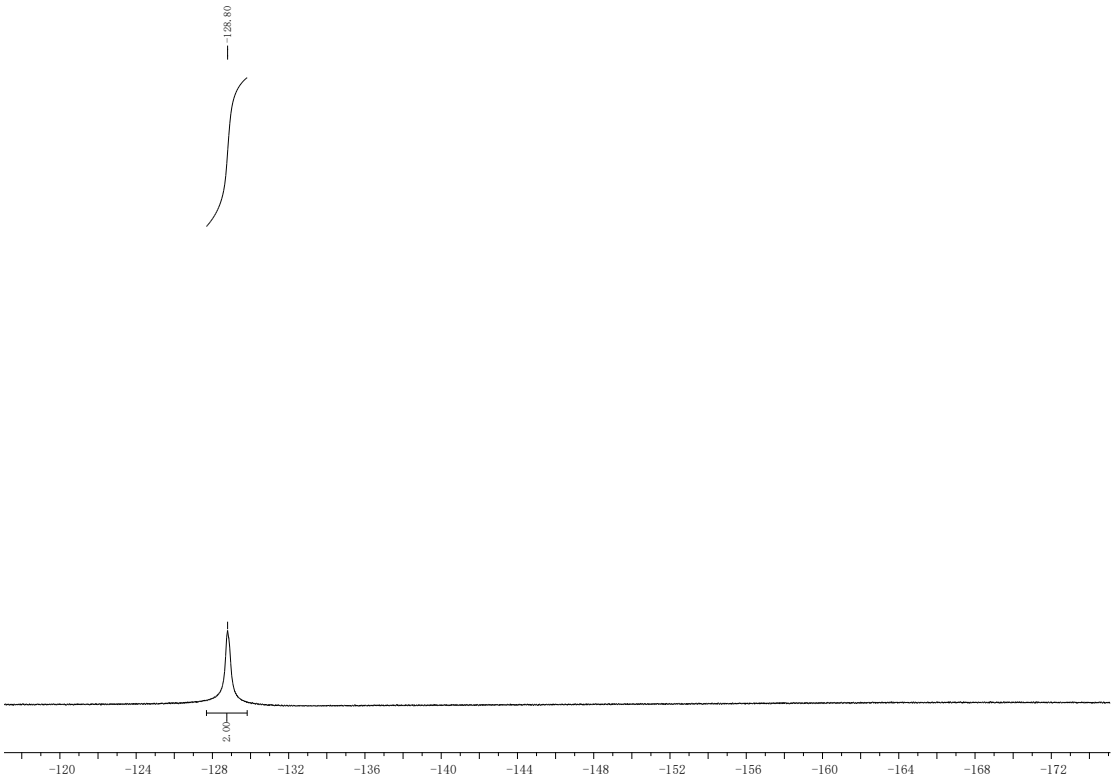

Fig. S19. ^{19}F NMR spectrum of **3a** in $CDCl_3$ at 293 K.

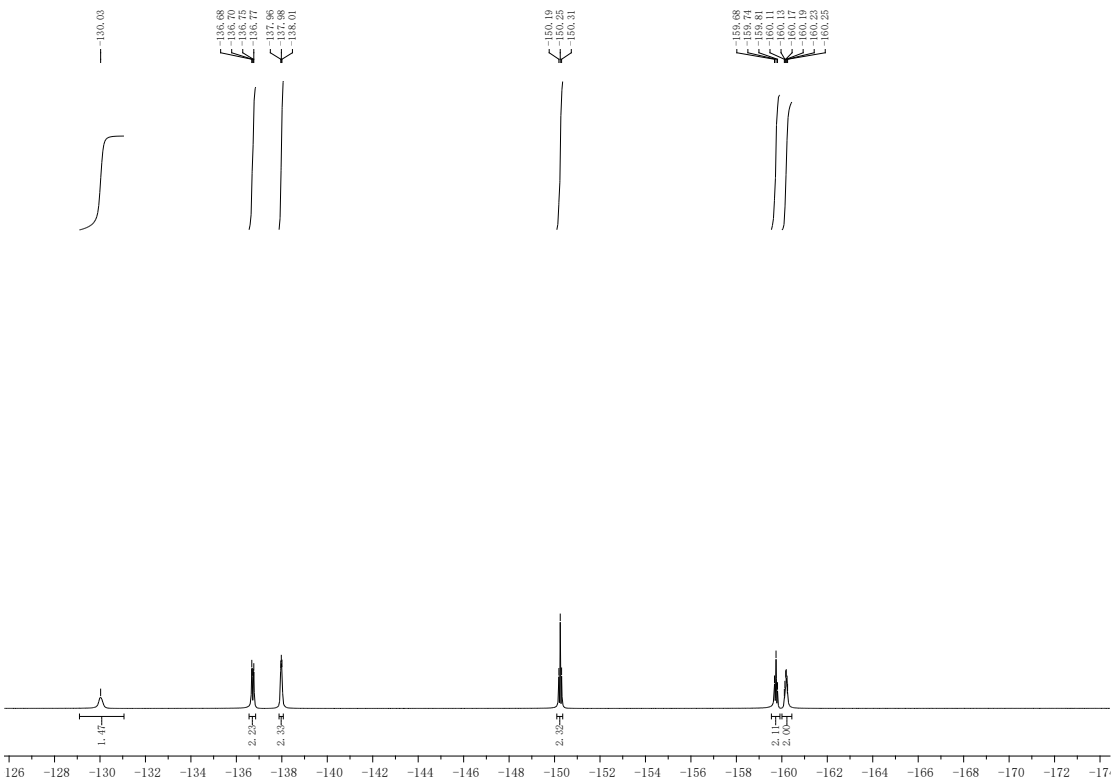

Fig. S20. ^{19}F NMR spectrum of **3b** in $CDCl_3$ at 293 K.

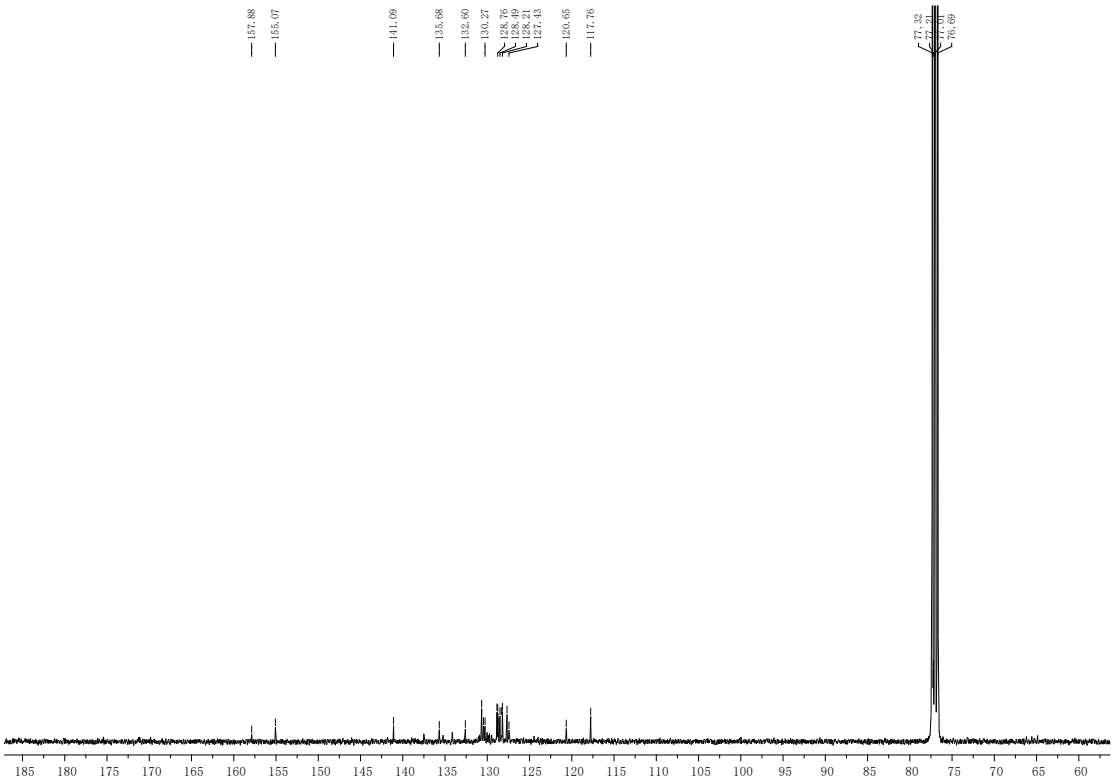

Fig. S21. ^{13}C NMR spectrum of **2a** in $CDCl_3$ at 293 K.

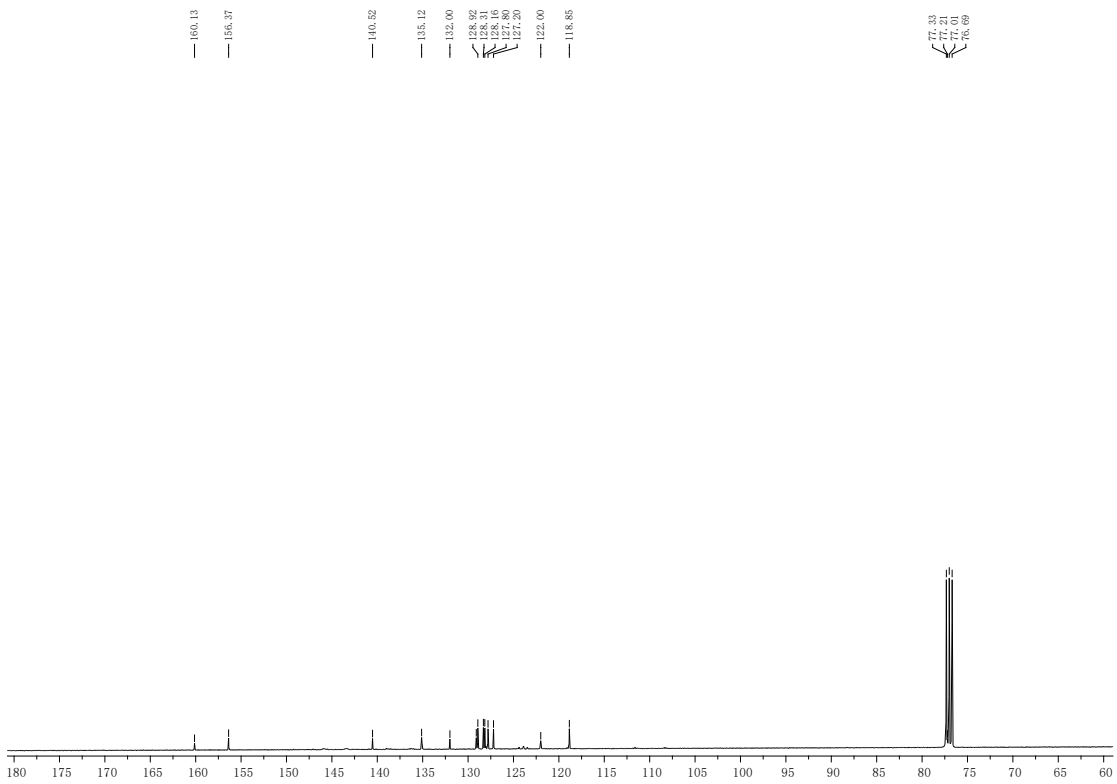

Fig. S22. ^{13}C NMR spectrum of **2b** in $CDCl_3$ at 293 K.

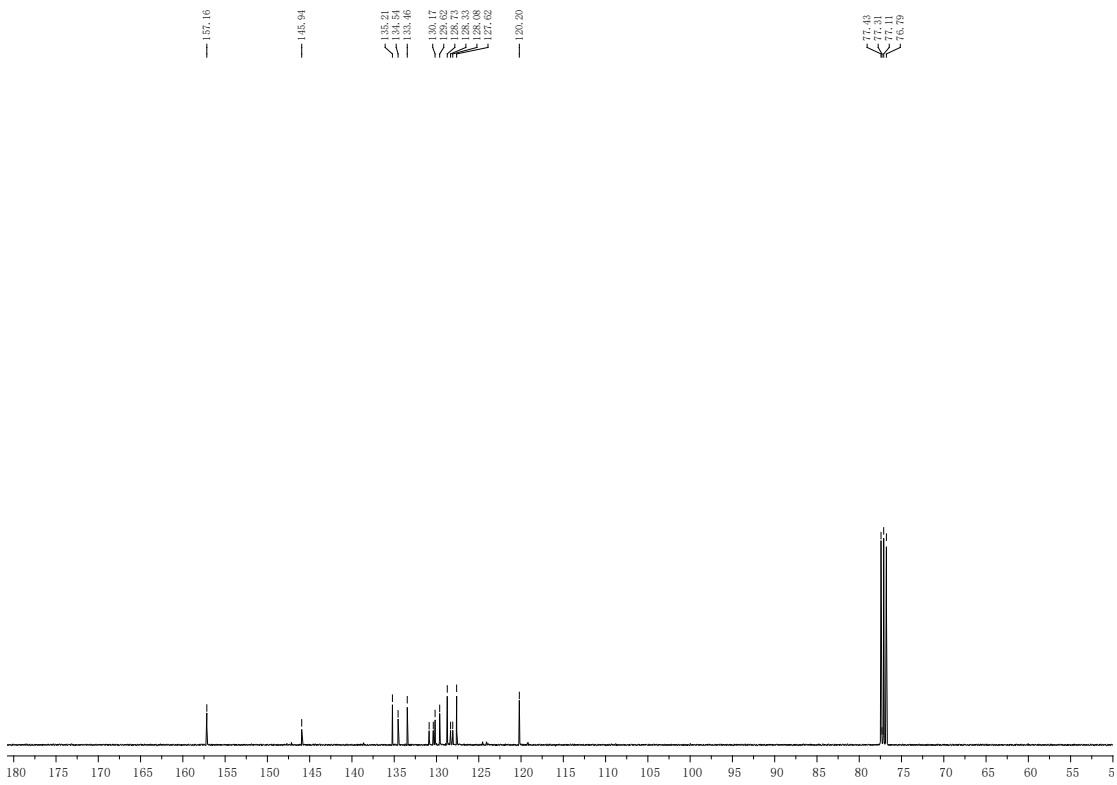

Fig. S23. ^{13}C NMR spectrum of **3a** in $CDCl_3$ at 293 K.

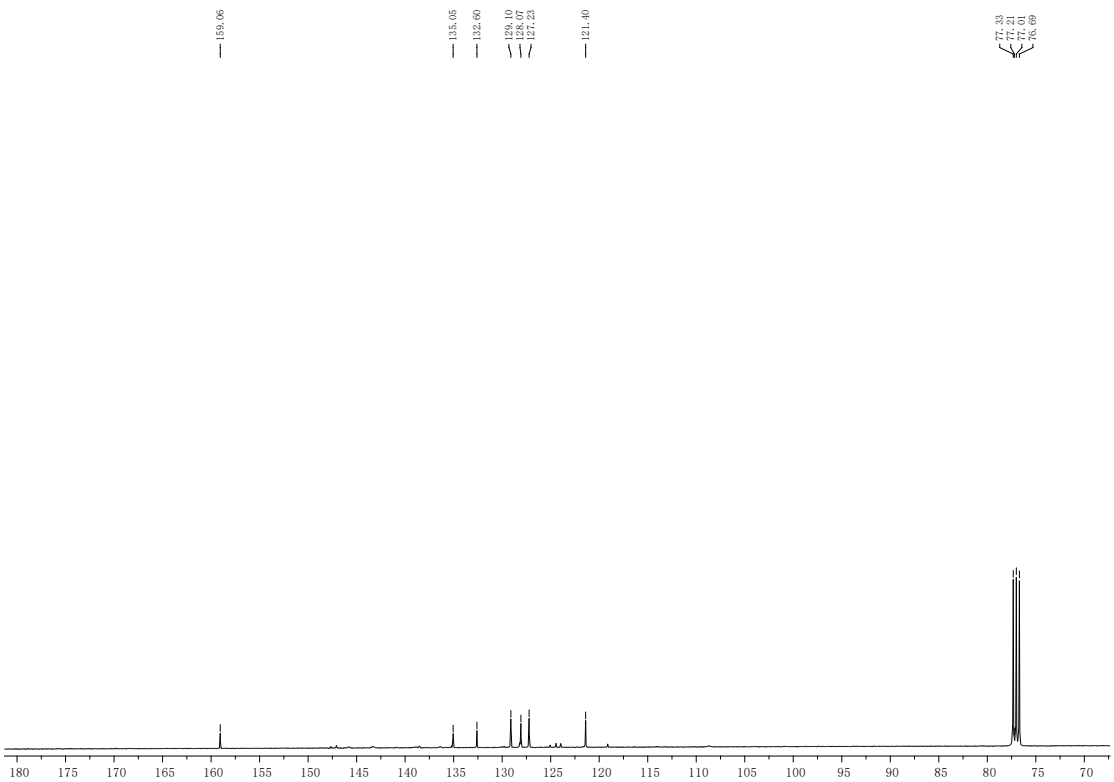

Fig. S24. ^{13}C NMR spectrum of **3b** in $CDCl_3$ at 293 K.

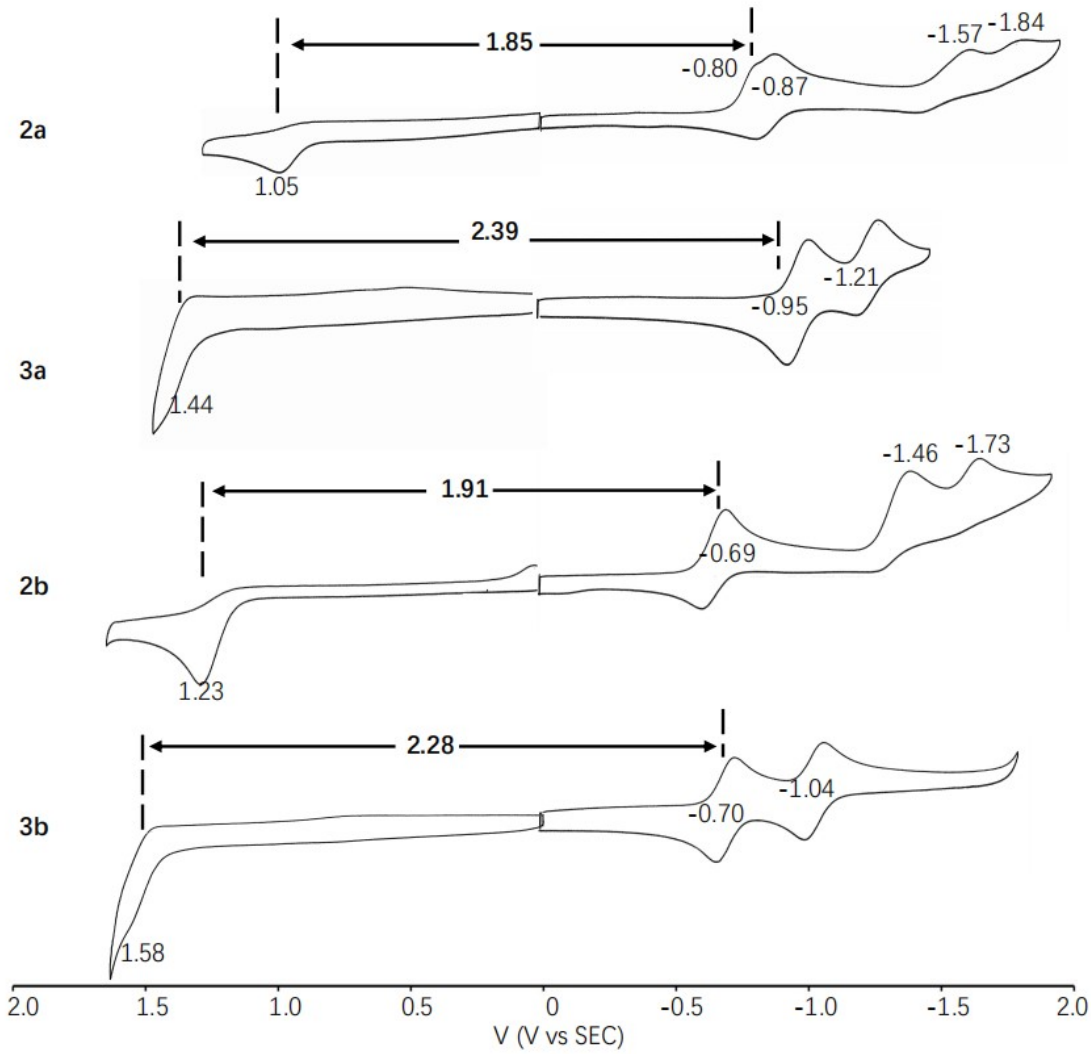

Fig. S25. CV of **2a**, **3a**, **2b**, and **3b** in CH_2Cl_2 with 0.1 M TBAP. Scan rate = 0.1 V s^{-1}.

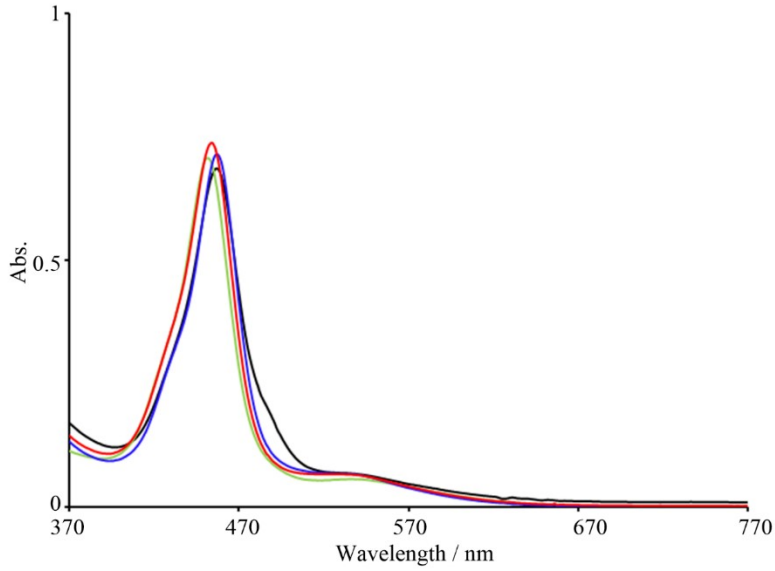

Fig. S26. UV-Vis absorption spectra of **2a** in hexane (green line), toluene (blue line), THF (red line), and $CHCl_3$ (black line).

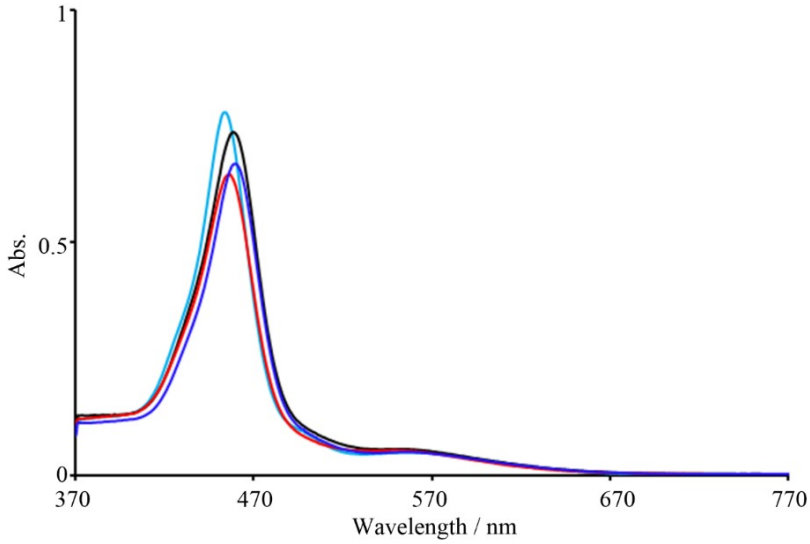

Fig. S27. UV-Vis absorption spectra of **2b** in hexane (green line), toluene (blue line), THF (red line), and $CHCl_3$ (black line).

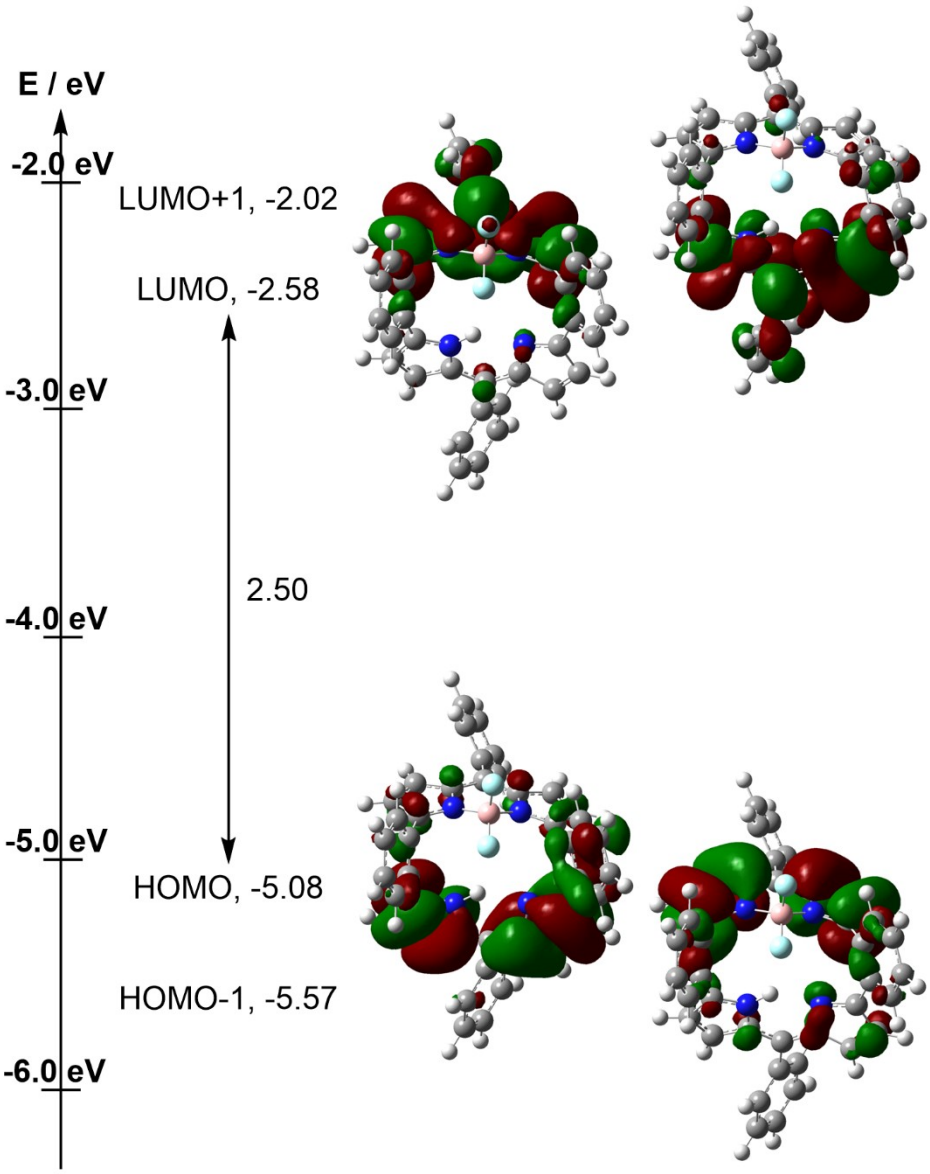

Fig. S28. Frontier molecular orbitals and energy diagrams of **2a**, calculated at the B3LYP/6-31G(d, p) level of theory.

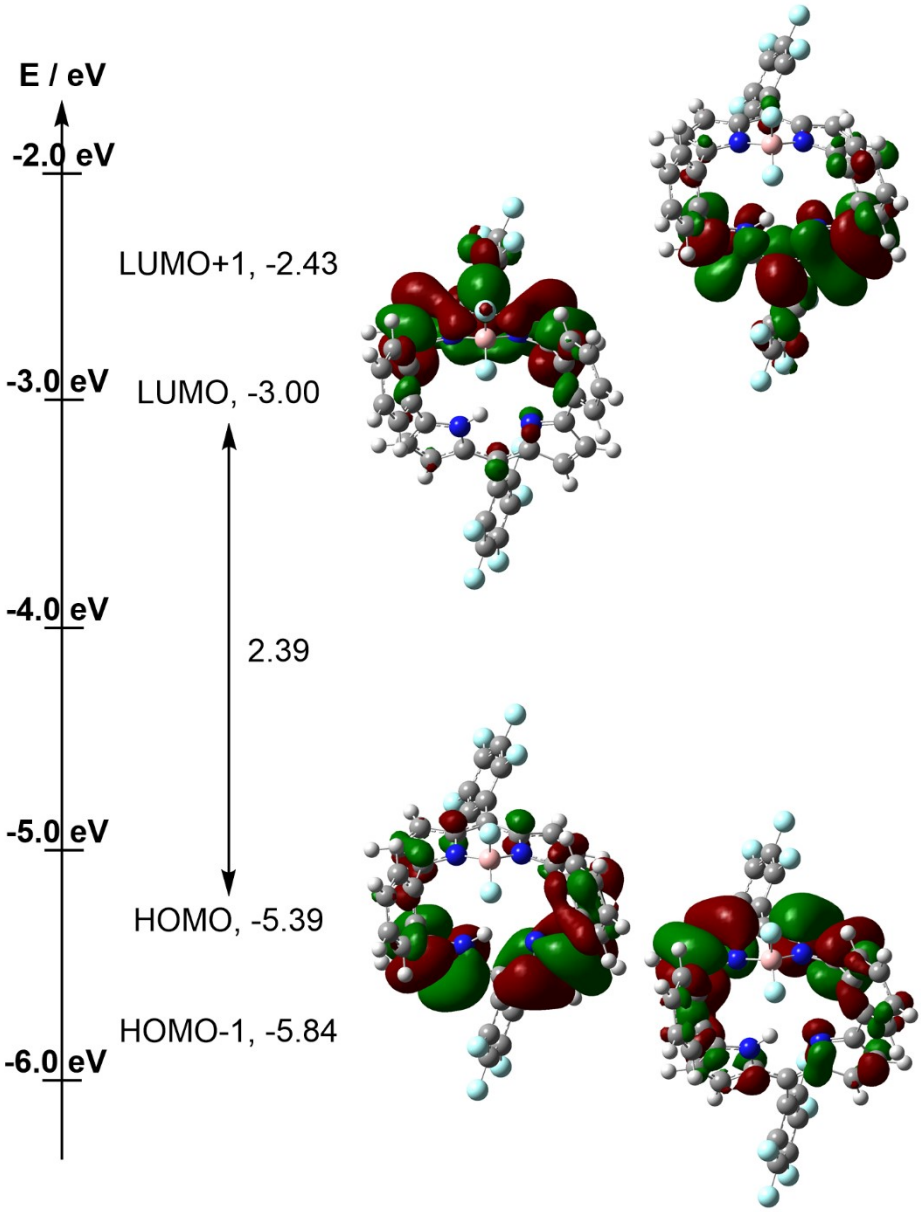

Fig. S29. Frontier molecular orbitals and energy diagrams of **2b**, calculated at the B3LYP/6-31G(d, p) level of theory.

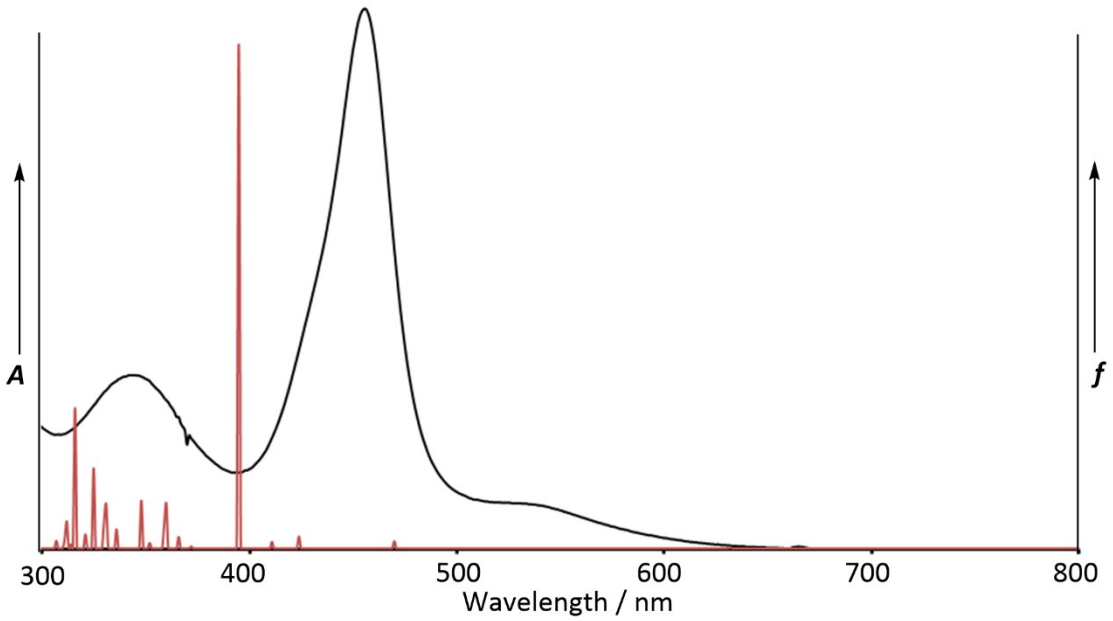

Fig. S30. The UV-Vis absorption spectrum (black line, left axis) and oscillator The UV-Vis absorption spectrum (black line, left axis) and oscillator strengths (red bar, right axis), which is calculated at the B3LYP/6-31G(d, p) level of theory of **2a**.

Table S1. Major composition, vertical excitation energies (*E*, eV/nm), and oscillator strengths (*f*) for the lowest optically allowed excited states of **2a**, calculated at the B3LYP/6-31G(d, p) level of theory.

State	**Major Composition**	**Exci.** (eV/nm)	*f*
1	H* -> L (0.70565)	1.96/631.92	0.0022
2	H-1 -> L (0.52898) H -> L+1 (0.44183)	2.64/469.71	0.0108
3	H-2 -> L (0.67550) H -> L+1 (0.11487) H-1 -> L+1 (0.15261)	2.93/423.59	0.0178
4	H -> L+1 (0.50985) H-1 -> L (-0.38830)	3.14/394.50	0.7417

*: H = HOMO, Highest Occupied Molecular Orbital, L = LUMO： Lowest Unoccupied Molecular Orbital.

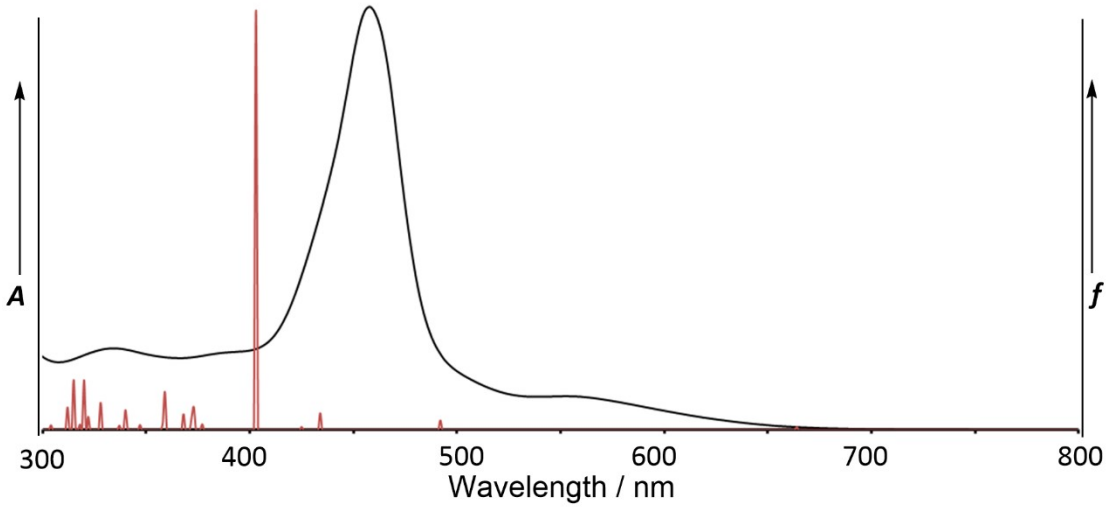

Fig. S31. The UV-Vis absorption spectrum (black line, left axis) and oscillator strengths (red bar, right axis), which is calculated at the B3LYP/6-31G(d, p) level of theory of **2b**.

Table S2. Major composition, vertical excitation energies (*E*, eV/nm), and oscillator strengths (*f*) for the lowest optically allowed excited states of **2b**, calculated at the B3LYP/6-31G(d, p) level of theory.

State	**Major Composition**	**Exci.** (eV/nm)	*f*
1	H* -> L (0.70455)	1.87/664.73	0.0056
2	H-1 -> L (54408) H -> L+1 (-0.41744)	2.52/492.18	0.0171
3	H-1 -> L+1 (0.54678) H-2 -> L (0.38513)	2.85/434.7	0.0297
4	H -> L+1 (0.51916) H-1 -> L (35954)	3.08/403.1	0.7280

*: H = HOMO, Highest Occupied Molecular Orbital, L = LUMO： Lowest Unoccupied Molecular Orbital.

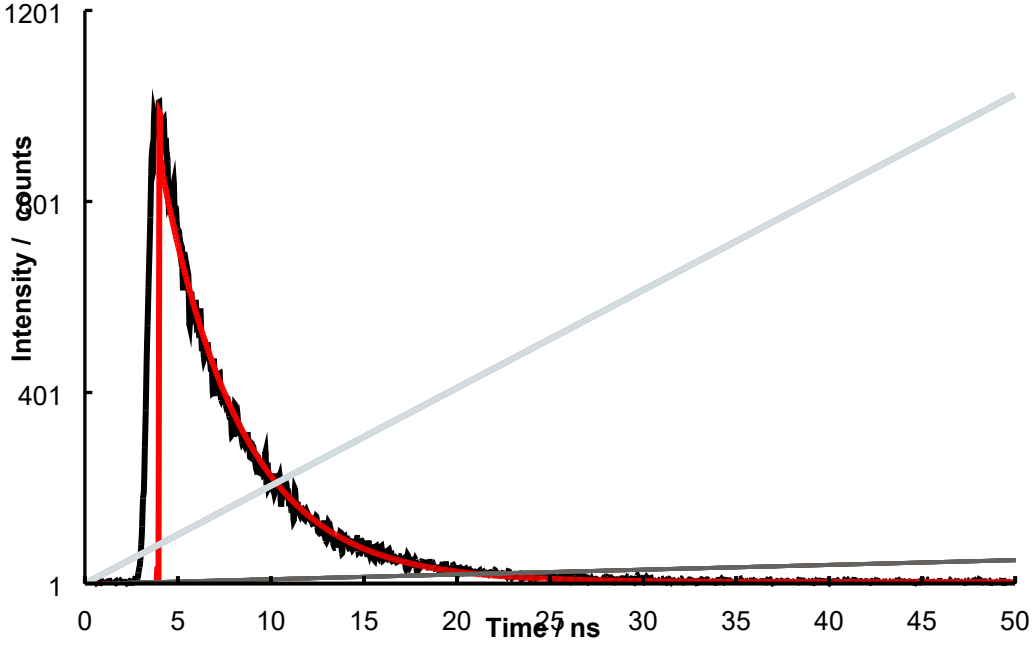

Fig. S32. Fluorescence decay profile of **3a** in toluene. Theoretical fits are also shown in red lines.

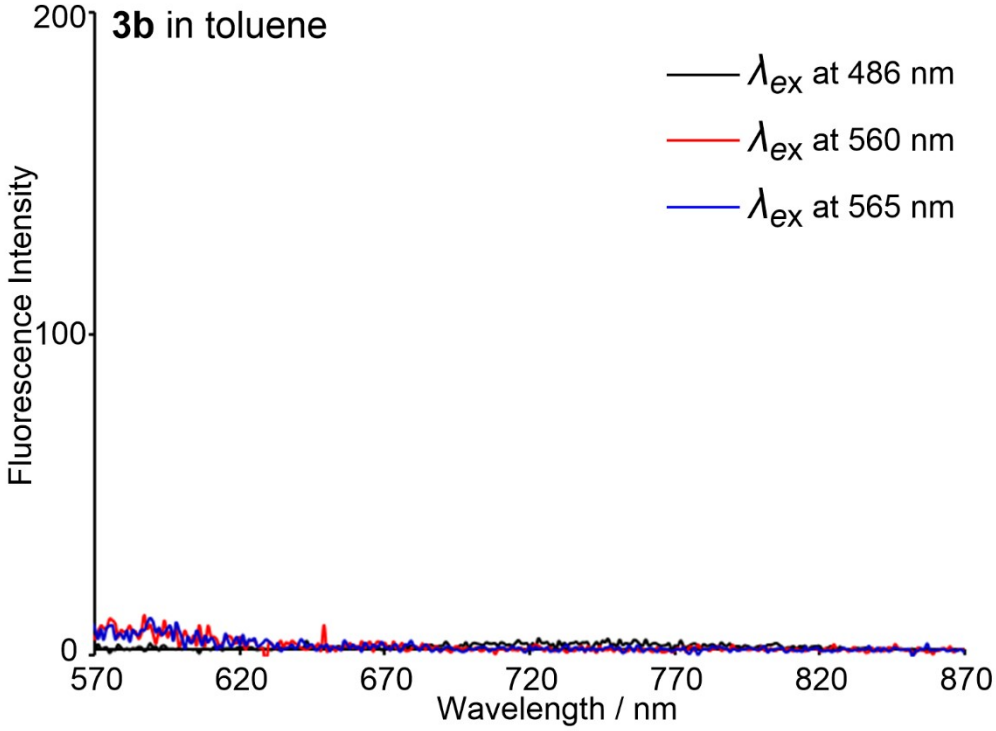

Fig. S33. Emission of **3b** in toluene.

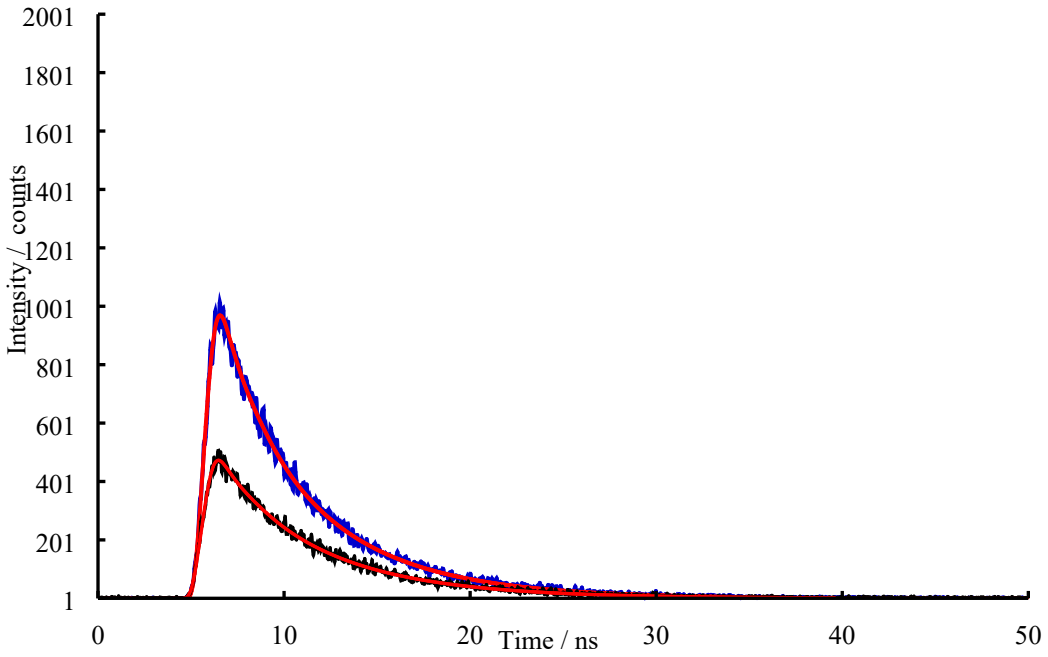

Fig. S34. Fluorescence decay profiles of **3b** in (a) solid (blue line) and (b) particle states (in THF/H_2O = 1/9, black line). Theoretical fits are also shown in red lines.

Table S3. Optical Properties of **2a**, **2b**, **3a,** and **3b**.

Cpd	λ_{abs}/nm in DCM (ε/mol^{-1}m^{5}cm^{-1})	λ_{em}/nm	Φ_F	τ/ns
2a	456(0.795) 534(0.068)	N/A	N/A	N/A
2b	460(0.890) 563(0.067)	N/A	N/A	N/A
3a	452(0.124) 475(0.846)	585 in toluene	0.022	4.32
3b	461(0.174) 486(1.003)	N/A in THF 680 (solid) 648 (THF/H_2O=1/9)	N/A in THF 0.015 (solid) 0.002 (THF/H_2O=1/9)	N/A in THF, 1.9 (34%), 5.5 (66%) (solid) 1.9 (22%), 5.7 (78%) (THF/H_2O=1/9)

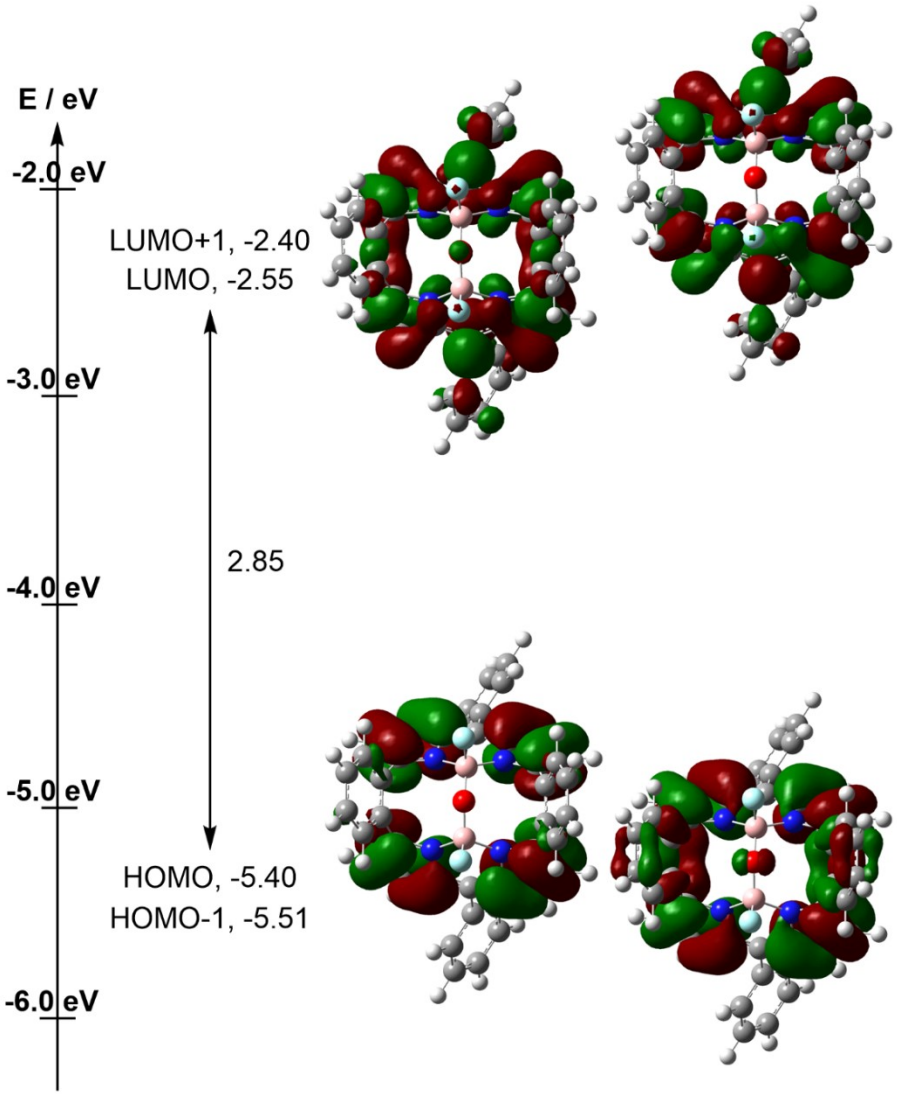

Fig. S35. Frontier molecular orbitals and energy diagrams of **3a**, calculated at the B3LYP/6-31G(d, p) level of theory.

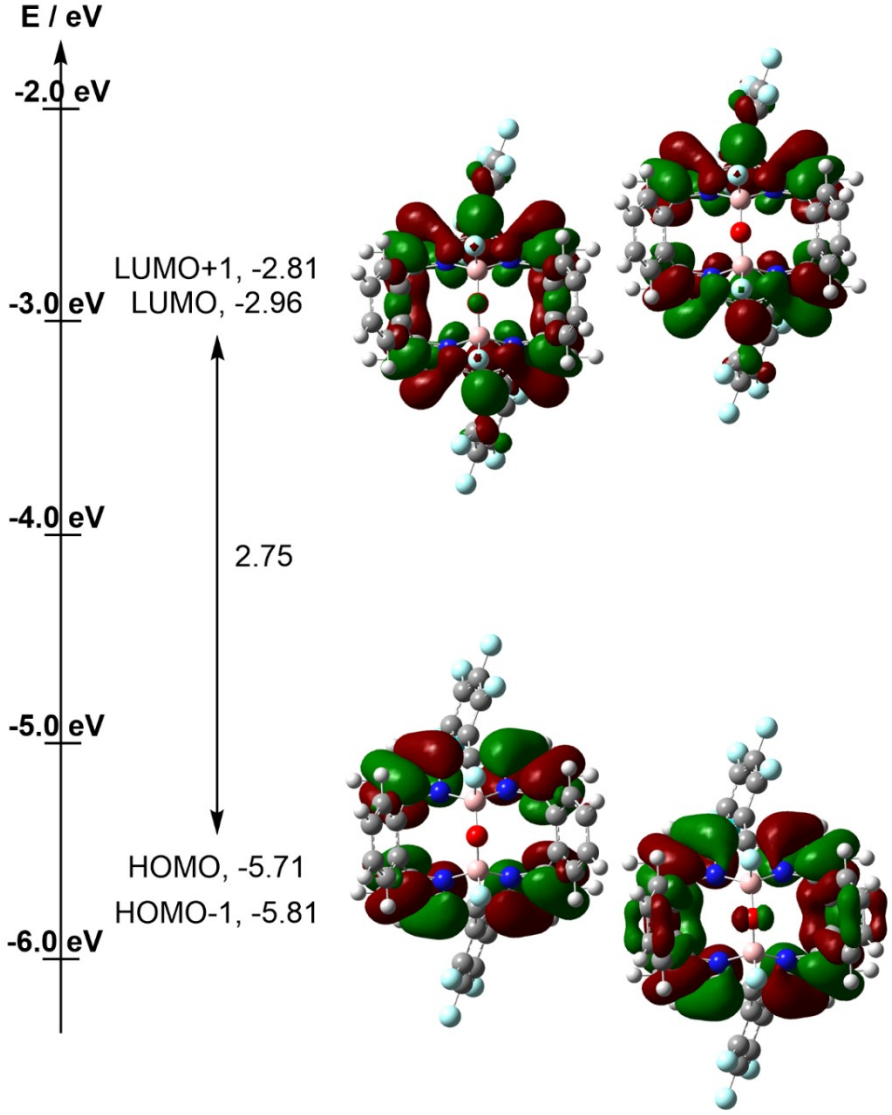

Fig. S36. Frontier molecular orbitals and energy diagrams of **3b**, calculated at the B3LYP/6-31G(d, p) level of theory.

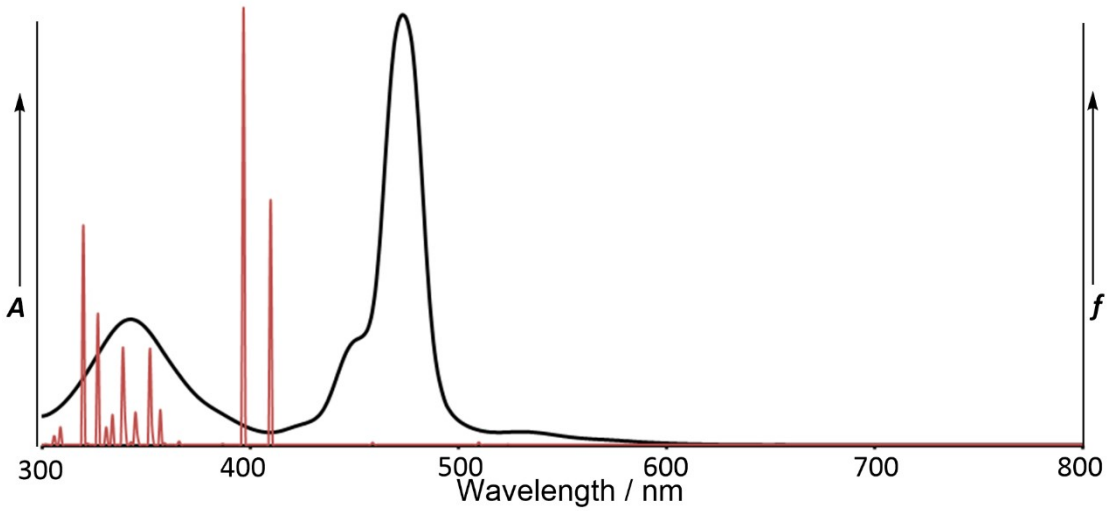

Fig. S37. The UV-Vis absorption spectrum (black line, left axis) and oscillator The UV-Vis absorption spectrum (black line, left axis) and oscillator strengths (red bar, right axis), which is calculated at the B3LYP/6-31G(d, p) level of theory of **3a**.

Table S4. Major composition, vertical excitation energies (*E*, eV/nm), and oscillator strengths (*f*) for the lowest optically allowed excited states of **3a**, calculated at the B3LYP/6-31G(d, p) level of theory.

State	Major Composition	Exci. (eV/nm)	*f*
1	H-1 -> L+1 (0.23868) H* -> L (0.66460)	2.36/524.45	0.0004
2	H-1 -> L (0.52845) H -> L+1 (0.46910)	2.43/510.48	0.0024
3	H -> L (-0.23037) H-1 -> L+1 (0.65708)	2.70/458.82	0.0021
4	H-2 -> L (0.55237) H-1 -> L (-0.27531) H -> L+1 (0.33086)	3.02/410.54	0.2505
5	H-2 -> L (0.42346) H-1 -> L (0.34732) H -> L+1 (-0.37657)	3.12/397.0	0.4472

*: H = HOMO, Highest Occupied Molecular Orbital, L = LUMO： Lowest Unoccupied Molecular Orbital.

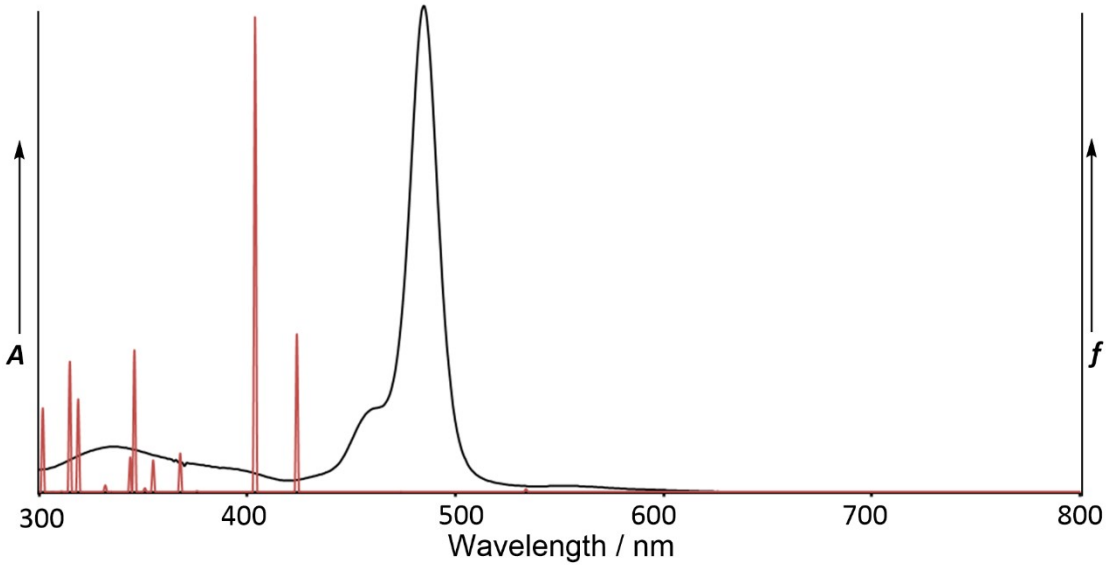

Fig. S38. The UV-Vis absorption spectrum (black line, left axis) and oscillator The UV-Vis absorption spectrum (black line, left axis) and oscillator strengths (red bar, right axis), which is calculated at the B3LYP/6-31G(d, p) level of theory of **3b**.

Table S5. Major composition, vertical excitation energies (*E*, eV/nm), and oscillator strengths (*f*) for the lowest optically allowed excited states of **3b**, calculated at the B3LYP/6-31G(d, p) level of theory.

State	**Major Composition**	**Exci.** (eV/nm)	***f***
1	H-1 -> L+1 (-0.28344) H* -> L (0.64720)	2.27/545.37	0.0001
2	H-1 -> L (0.53196) H -> L+1 (-0.46511)	2.32/534.21	0.0031
3	H-2 -> L+1 (0.59801) H-1 -> L (-0.22973) H -> L+1 (-0.28755)	2.92/424.62	0.1699
4	H -> L+1 (0.40718) H-1 -> L (0.36753) H-2 -> L (0.35196)	3.07/404.29	0.5112

*: H = HOMO, Highest Occupied Molecular Orbital, L = LUMO： Lowest Unoccupied Molecular Orbital.

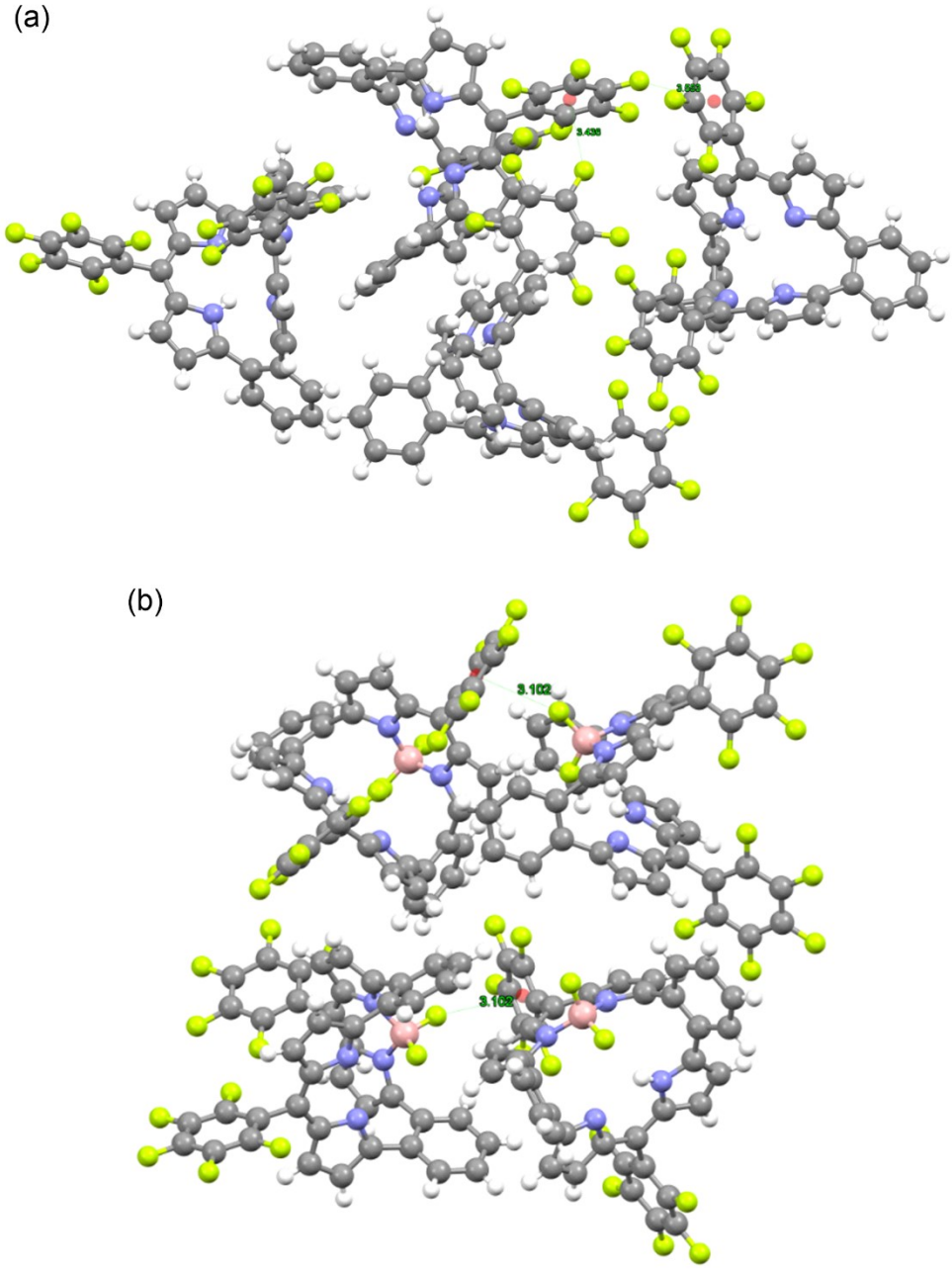

Fig. S39. Packing structure and selective distances (Å) of (a) **1b** and (b) **2b** in the crystal structure. The data of **1b** was taken from ref. 3c.

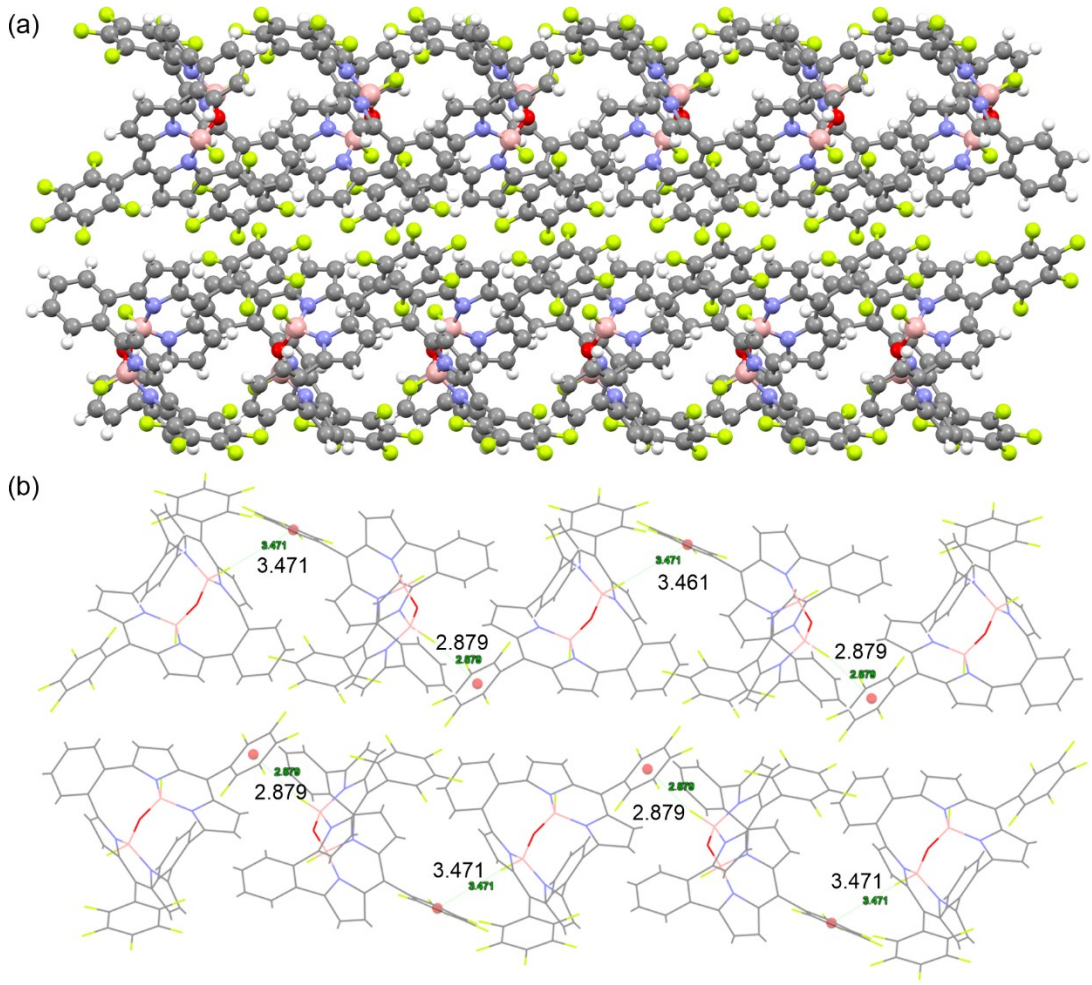

Fig. S40. (a) One view (b-axis) and the secondary interaction (F-π) (Å) of the packing structures of **3b** were observed in the crystal structure.

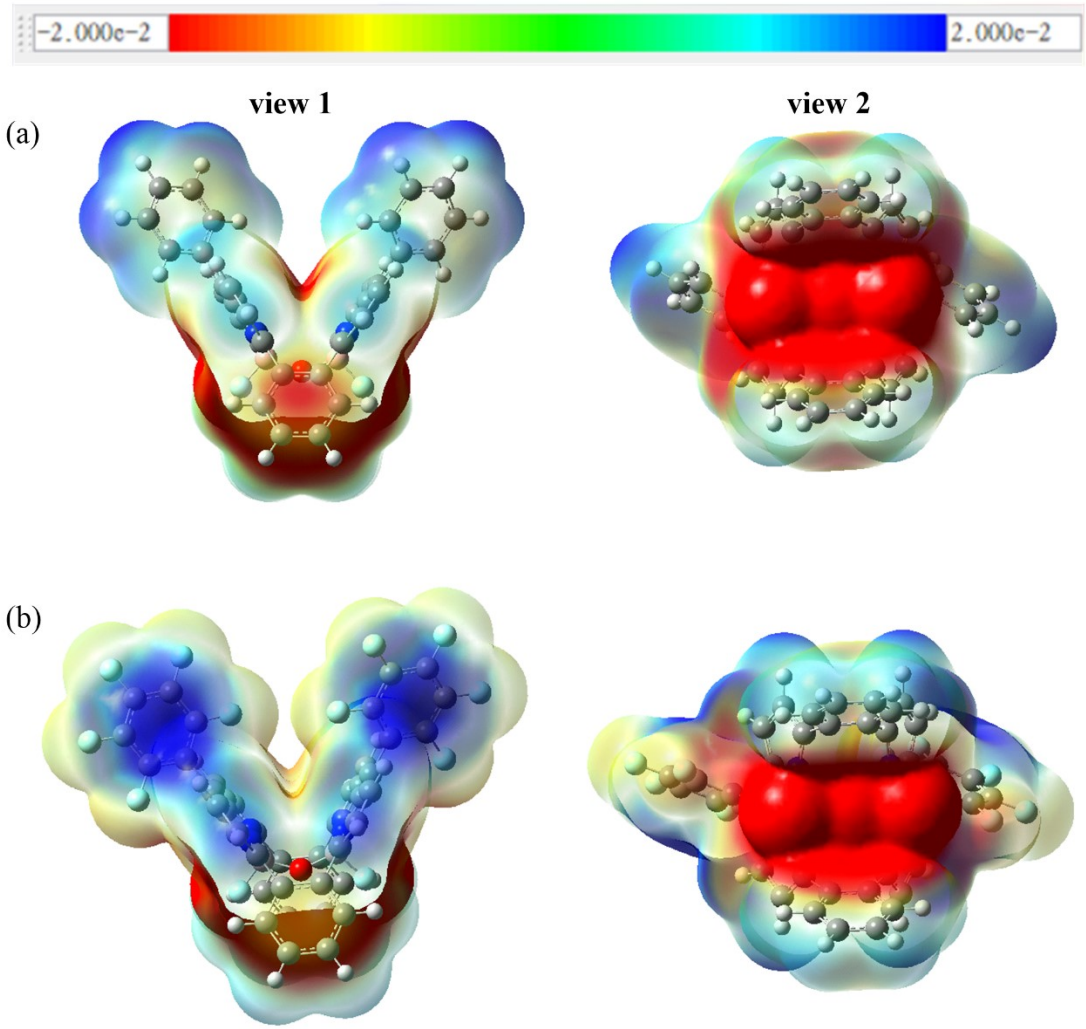

Fig. S41. Electrostatic potential surfaces of (a) **3a** and (b) **3b**.

5. Crystal Data

Table S6. Crystal data of **2a**

Empirical formula	$C_{42}H_{27}BF_2N_4$, 3(CH_3OH)
Formula weight	732.61
Temperature/*K*	213.00
Crystal system	monoclinic
Space group	$P2_1/c$
Unit cell dimensions	a = 15.6793(5) Å
	b = 15.5603(6) Å β = 106.768(2)°
	c = 16.0167(5) Å
Volume/Å^3	3741.5(2)
Z	4
ρ_{calc}g/cm^3	1.301
μ/mm^{-1}	0.457
F(000)	1536
Crystal size/mm^3	0.05 × 0.02 × 0.01
Radiation	GaKα (λ = 1.34139)
Theta range for data collection/°	3.522 to 45.023
Index ranges	$-19 \leq h \leq 19$, $-18 \leq k \leq 18$, $-19 \leq l \leq 19$
Reflections collected	33224
Independent reflections	7016 [R_{int} = 0.1013]
Data/restraints/parameters	7106/0/442
Goodness-of-fit on F^2	1.024
Final R indexes [$I >= 2\sigma(I)$]	R_1 = 0.0852, wR_2 = 0.2208
Final R indexes [all data]	R_1 = 0.1693, wR_2 = 0.2728
Largest diff. peak/hole / e Å^{-3}	0.27/-0.34

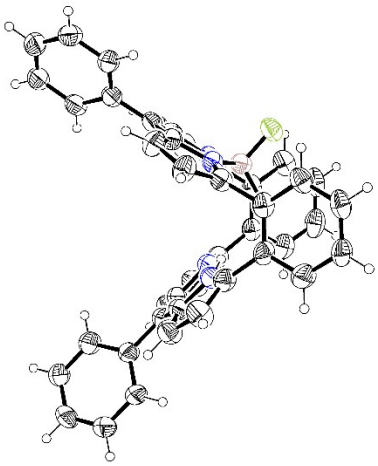

Fig. S42. Crystal structure of **2a**. The thermal ellipsoids represent a 40% probability.

Table S7. Crystal data of **3a**

Empirical formula	$C_{44}H_{34}B_2F_2N_4O_3$, 0.5($CHCl_3$)

Formula weight	721.97
Temperature/*K*	193.00
Crystal system	monoclinic
Space group	$P2_{1/c}$
Unit cell dimensions	a = 18.948(12) Å
	b = 13.024(7) Å β = 110.339(17)°
	c = 15.721(9) Å
Volume/Å^3	3638(2)
Z	4
ρ_{calc}g/cm^3	1.318
μ/mm^{-1}	0.192
F(000)	1484.0
Crystal size/mm^3	0.12 × 0.1 × 0.1
Radiation	MoKα (λ = 0.71073)
Theta range for data collection/°	2.087 to 22.998
Index ranges	$-18 \leq h \leq 20$, $-14 \leq k \leq 14$, $-17 \leq l \leq 17$
Reflections collected	17472
Independent reflections	5071 [R_{int} = 0.0515]
Data/restraints/parameters	5071/276/503
Goodness-of-fit on F^2	1.033
Final R indexes [I>=2σ (I)]	R_1 = 0.0630, wR_2 = 0.1614
Final R indexes [all data]	R_1 = 0.1073, wR_2 = 0.1923
Largest diff. peak/hole / e Å^{-3}	0.270/-0.266

Even two fluorine atoms refine to an occupancy of 92% and 90%, but the structure of this complex has been proved by HR-MS, ^{1}H NMR and ^{19}F NMR without any doubt. It's possible to happen these fluorine atoms positions can be exchanged for oxygen atoms because MeOH has been used to make crystals of **3a**.[4]

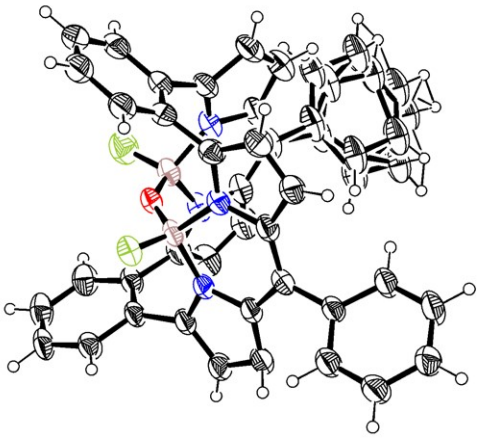

Fig. S43. Crystal structure of **3a**. The thermal ellipsoids represent a 50% probability.

Table S8. Crystal data of **2b**

Empirical formula	$C_{43}H_{19}BF_{12}N_4Cl_2$, CH_2Cl_2
Formula weight	901.33

Temperature/*K*	193.00
Crystal system	orthorhombic
Space group	*Pbca*
Unit cell dimensions	a = 15.0470(13) Å
	b = 19.8971(17) Å
	c = 26.914(2) Å
Volume/Å^3	8057.7(12)
Z	8
ρ_{calc}g/cm^3	1.486
μ/mm^{-1}	1.496
F(000)	3616.0
Crystal size/mm^3	0.12 × 0.1 × 0.1
Radiation	GaKα (λ = 1.34139)
Theta range for data collection/°	3.508 to 58.195
Index ranges	$-19 \leq h \leq 19$, $-25 \leq k \leq 25$, $-34 \leq l \leq 34$
Reflections collected	82903
Independent reflections	9019 [R_{int} = 0.0825]
Data/restraints/parameters	9019/0/532
Goodness-of-fit on F^2	1.014
Final R indexes [$I >= 2\sigma(I)$]	R_1 = 0.0511, wR_2 = 0.1331
Final R indexes [all data]	R_1 = 0.0963, wR_2 = 0.1588
Largest diff. peak/hole / e Å^{-3}	0.185/-0.245

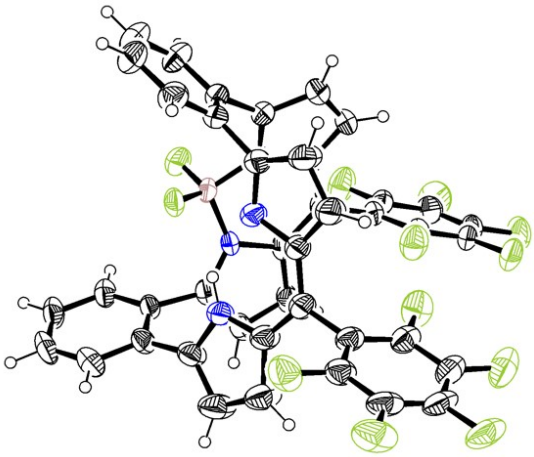

Fig. S44. Crystal structure of **2b**. The thermal ellipsoids represent a 50% probability.

Table S9. Crystal data of **3b**

Empirical formula	$C_{42}H_{16}B_2F_{12}N_4O$
Formula weight	842.21
Temperature/*K*	193.00

Crystal system	monoclinic
Space group	P21/c
Unit cell dimensions	a = 21.3588(18) Å
	b = 11.3229(8) Å β = 92.765(4)°
	c = 14.4859(11) Å
Volume/Å^3	3499.2(5)
Z	4
ρ_{calc}g/cm^3	1.599
μ/mm^{-1}	0.789
F(000)	1688.0
Crystal size/mm^3	0.12 × 0.1 × 0.1
Radiation	GaKα (λ = 1.34139)
Theta range for data collection/°	3.604 to 120.728
Index ranges	$-27 \leq h \leq 19$, $-14 \leq k \leq 10$, $-18 \leq l \leq 17$
Reflections collected	27005
Independent reflections	7693 [R_{int} = 0.0532, R_{sigma} = 0.0467]
Data/restraints/parameters	7693/0/550
Goodness-of-fit on F^2	1.046
Final R indexes [$I >= 2\sigma(I)$]	R_1 = 0.0473, wR_2 = 0.1222
Final R indexes [all data]	R_1 = 0.0770, wR_2 = 0.1385
Largest diff. peak/hole / e Å^{-3}	0.35/–0.33

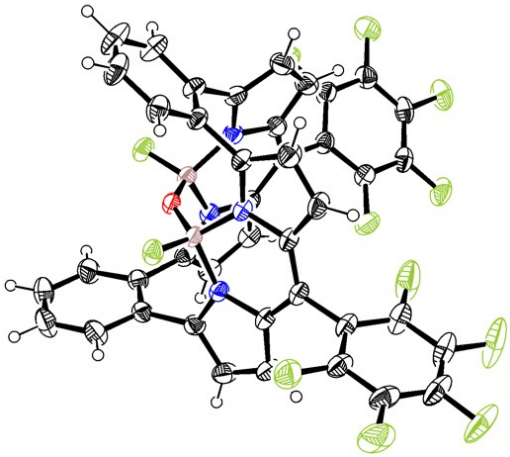

Fig. S45. Crystal structure of **3b**. The thermal ellipsoids represent a 50% probability.

6. References

(1) Gaussian 09, Revision B.01, M. J. Frisch, G. W. Trucks, H. B. Schlegel, G. E. Scuseria, M. A. Robb, J. R. Cheeseman, G. Scalmani, V. Barone, B. Mennucci, G. A. Petersson, H. Nakatsuji, M. Caricato, X. Li, H. P. Hratchian, A. F. Izmaylov, J. Bloino,

G. Zheng, J. L. Sonnenberg, M. Hada, M. Ehara, K. Toyota, R. Fukuda, J. Hasegawa, M. Ishida, T. Nakajima, Y. Honda, O. Kitao, H. Nakai, T. Vreven, J. A. Montgomery, Jr., J. E. Peralta, F. Ogliaro, M. Bearpark, J. J. Heyd, E. Brothers, K. N. Kudin, V. N. Staroverov, T. Keith, R. Kobayashi, J. Normand, K. Raghavachari, A. Rendell, J. C. Burant, S. S. Iyengar, J. Tomasi, M. Cossi, N. Rega, J. M. Millam, M. Klene, J. E. Knox, J. B. Cross, V. Bakken, C. Adamo, J. Jaramillo, R. Gomperts, R. E. Stratmann, O. Yazyev, A. J. Austin, R. Cammi, C. Pomelli, J. W. Ochterski, R. L. Martin, K. Morokuma, V. G. Zakrzewski, G. A. Voth, P. Salvador, J. J. Dannenberg, S. Dapprich, A. D. Daniels, O. Farkas, J. B. Foresman, J. V. Ortiz, J. Cioslowski, and D. J. Fox, Gaussian, Inc., Wallingford CT, 2010.

(2) G. Sheldrick, *Acta Cryst.* **2008**, *A64,* 112.

(3) (a) S. Xue, D. Kuzuhara, N. Aratani,H. Yamada, *Org. Lett.* **2019**, *21,* 2069; (b) D. Kuzuhara, W. Furukawa, A. Kitashiro, N. Aratani, H. Yamada, *Chem. - Eur. J.* **2016**, *22,* 10671; (c) N. Liu, W. R. Osterloh, H. Huang, X. Tang, P. Mei, D. Kuzuhara, Y. Fang, J.Pan, H. Yamada, F. Qiu, K. M. Kadish, S. Xue, *Inorg. Chem.* **2022**, *61,* 3563.

(4) (a) R. E. Mesmer, A. C. Rutenberg, *Inorg. Chem.* **1973**, *12,* 699; (b) D. Feldman, D. Segal-Lew, M. Rabinovitz, *J. Org. Chem.* **1991**, *56,* 7350.